"Study of strain pattern in deep drawn square Aluminum cup"

Major Project Report

Submitted in Partial Fulfillment of the Requirements for
The Degree of

MASTER OF TECHNOLOGY
IN
MECHANICAL ENGINEERING
(CAD/CAM)

by

Dhaval Jethva
(05MME007)

Under the guidance of

Prof. B. A. Modi

Department of Mechanical Engineering
INSTITUTE OF TECHNOLOGY
NIRMA UNIVERSITY OF SCIENCE & TECHNOLOGY.
AHMEDABAD-382 481

May 2007

CERTIFICATE

This is to certify that the Major Project Report entitled **"Study of strain pattern in deep drawn square Aluminum cup"** submitted by **Dhaval Jethva (05MME007)** towards the partial fulfillment of the requirements for Master of Technology (Mechanical) in the field of CAD/CAM of Nirma University of Science and Technology is the record of work carried out by him under our supervision and guidance. The work submitted has in our opinion reached a level required for being accepted for examination. The results embodied in this major project work to the best of our knowledge have not been submitted to any other University or Institution for award of any degree or diploma.

Project Guide:

Prof. B. A. Modi.
Assistant professor,
Mechanical Engineering,
Institute of Technology.

Prof. V. R. Iyer.
Head of Department,
Mechanical Engineering,
Institute of Technology.

Prof. A. B. Patel.
Director,
Institute of Technology,
Nirma University of Science and Technology.

Examiners

1)

2)

3)

4)

Abstract

This report is aimed to study the different strain pattern in the deep drawn square Aluminum cup. In the automotive industry, significant efforts are being put forth to replace steel sheet with Aluminum alloy. Study of square cup deep drawing can help to study the strain pattern in the complicated geometry shape also. There are different material and processing parameters on which the result of the deep drawing process depends. The performance measure of the deep drawing process is flow limit diagram which shows the major and minor strains.

It this project effect of different materials and processing parameters affecting deep drawing have been studied. Binder force is required for the deep drawing without failure of the component. That is determined by R_{off} value technique. It takes care of all the parameters affecting deep drawing.

FEA simulations for deep drawing of square cup (50x25x25) are carried out with material as pure aluminum (1100). The simulations are carried out with three different shaped blanks. Minimum strain has been noticed with square blank with corner radius. With same methodology simulations for the aluminum alloy (5052) have been carried out with two different die radiuses. Flow limit diagrams of the above simulations were carried out to study the strain pattern. Macro has been developed in ANSYS parametric design language (*APDL*) to carry out the above simulations. It reduces the time required for the simulation.

Experimental validation for the deep drawn cup of pure aluminum (1100) has been carried out. Die set is designed for the experiment. Circular grid pattern is marked on the blank to study the strain pattern of deep drawn cup. Laser marking method is used for grid marking. Measurements of the minor and major strains have been carried out on the profile projector. Flow limit curves from the experimental results have been drawn. Simulated results and experimental results are in very good agreement.

Key words: R_{off} value, Flow limit diagram, Major strain, Minor strain, Macro APDL, Laser grid marking.

Acknowledgement

It is indeed pleasure for me to express my sincere gratitude to those who have always helped me through my project work.

First of all I would like to thank my project guide **Prof. B. A. Modi** who helps me selecting project topic, understanding of the subject, stimulating suggestions, encouragement and also for writing of this thesis. I am sincerely thankful for their valuable guidance and help to enhance my presentation skills.

I would also like to thank our head of the department **Prof. V. R. Iyer** for providing valuable guidance and also to the management of Nirma Education and Research Foundation (NERF) for providing excellent infrastructure and facilities whenever and wherever required.

I would also like to thank **Sahajanand Laser pvt. ltd**, and **Jayantilal Ratilal Punchal** and **Rakesh Jayantilal Punchal** for helping me to carried out experiment.

Finally, I am thankful to all the faculty member of Mechanical Engineering Department, Laboratory assistants, Library staff and all my friends, colleagues who have directly or indirectly helped me during this project work.

Date /05/07.

Dhaval Jethva
(05mme007)
M.Tech. (CAD/CAM)

Contents

List of Figures

List of Tables

Nomenclature

ρ_d	Die radii.
n	Strain hardening coefficient.
B_1	Blank size measured from the center of the blank.
B_2	Punch size measured from the center of the blank.
c	Punch die clearance.
Rp	Plan view radius.
ϴ	Plan view angle.
β1, β2	Plan view angles measured from the plain strain section.
dr	Die corner radii.
b	Blank clamped between binder and die.
pr	Punch radius.
α	Contact angle.
Bo	Half of the blank size of the base model.
Co	Punch die clearance of the base model.
Po	Punch size measured from the center of the blank.
p_{ro}	Punch radius of the base model.
Rpo	Plane view radius of the base model.
A1,A2	Contact area at the straight section of the die.
A3	Total contact area.
t	Thickness of the sheet metal.
Fb	Total binder force.
Fs	Side restraining force per unit length.
Fc	Corner restraining force per unit length.
μ	Interface friction coefficient.
ε_o	Center averaged principal strain.
Pd	Failure height of 3D model.
E	Young's Modulus.
r_{off}	Center offset.
S	Size of the model.
k	Draw ratio factor.
B	Averaged blank size.
d	Averaged draw ratio factor.

d_1	Draw ratio in direction of the 1st plane strain section.
d_2	Draw ratio in direction of the 2nd plane strain section.
d_0	Draw ratio of the base model.
Dc	Corner stretch height.
Ds	Averaged side stretch height.
Ds_1	Side stretch height along the 1st plane strain section.
Ds_2	Side stretch height along the 2nd plane strain section.
▲	Wall stretching difference.
б	Difference of restraining stress.
H	Offset modification parameter.
R	Radius of the analytical arc beam.
h	Height of the analytical arc beam.
Φ	Barlat's Yield function.
Si', Sj'	The principal values of the linear transformations on the stress deviator.
a	Barlat's exponent.

CHAPTER 1
Introduction

1.1 Introduction

Sheet metal forming is most widely used manufacturing processes for the wide range of products in many industries. In the automotive industry, significant efforts are being put forth to replace steel sheet with aluminum sheet alloys for automotive application. Lighter in weight, aluminum sheets would improve the fuel efficiency of the vehicles. However, besides higher material cost, there are several technical hurdles to overcome for widespread use of the aluminum alloy sheets, such as lower formability and larger spring back compared to steel sheets

The reason behind the sheet metal forming is gaining a lot of attention in the modern technology is due to the ease with which metal is formed into useful shape by plastic deformation in which volume and mass of the metal is conserved and metal is deformed from one location to another. Deep drawing is extensively used process for the manufacturing for mass production of cup shape components in very short period of time. In deep drawing metal blank is deformed in to the die cavity by the action of punch and support of the die. Deep drawing products in modern industries have very complicated shape. So these have to go successive stage for the final shape. As due to very complicated shape the forces and the strain pattern is different at the different location. There are basically two things which create that difference, anisotropy of the materials and complicated geometry of the product. Due to that main area of concern is the strain in the different portion of the blank at the time of deformation. As there are many material and the processing parameters which have to consider for the optimization of the process.

Earing and wrinkles are highly undesirable defects in deep drawing which effects load and work required for the product. There are many parameters which affect the deep drawing process like die radius, punch radius, blank holding force, punch velocity, lubrication, die and punch clearance and many of that. So for the optimization of the process each and every parameter should be considered. If we consider the stain pattern in the square cup as the radius at the corner and the flat part have different strain pattern or we can say they will deform at the different stretching height and that is largely depends upon the center strain. Also difference in the major and minor strains creates wrinkle. As experimental process for finding the optimal result is very expensive and time so numerical simulation tools have been found as attractive alternative. FEM simulation of the process is also required fair amount of time for getting the simulation so to reduce time for carrying out different simulation macro has to be used for input of the processing and material parameters, for that Ansys parametric design language (APDL) can be used.

1.1.1 Analysis of deep drawing.

Two principal actions usually take place in deep drawing: (1) biaxial stretching over a punch, in which both principal strains are tensile, and (2) drawing of a flange into a die cavity in which one principle strain is tensile and other is compressive. [13]

For use in analysis of deep drawing, the flat blank may be divided into three zones, X, Y, Z as shown in fig.1.1 The outer annular zone X consists of material in contact with die, the inner annular zone Y is initially not in contact with either punch or the die, and the circular zone Z is in contact with die bottom of the punch only.

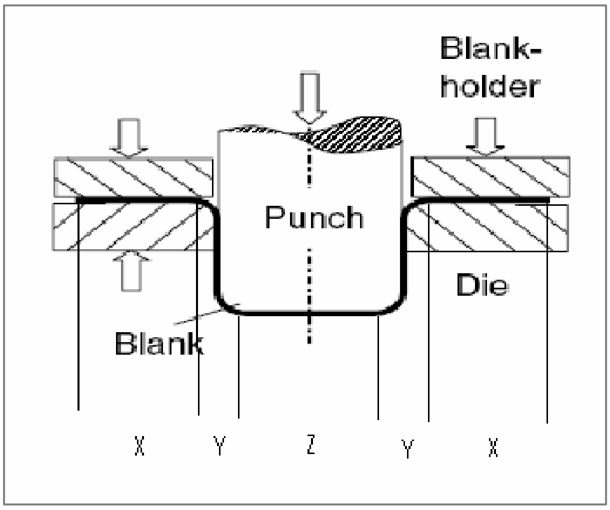

Fig: 1.1 Initial stages of deep drawing

During the course of deep drawing, the following five processes take place:

1. Pure radial drawing between the die and blank holder.
2. Bending and sliding over the die profile.

3. Stretching between the die and punch.
4. Bending and sliding over the punch profile.
5. Stretching and sliding over the punch nose.

Various parts of zone X may go through some or all of the process 1, 2, 3; those of Y through 2, 3, and 4; and those of Z through 3, 4, and 5. The first process thickens the metal, and 3 and 5 thin it.

1.2 Aim of the project.

Due to the complexity of the geometry in the square cup at the strain pattern in the different zone creates the wrinkles and earing which is not required in the final product and it also increases the processing work load and time. As due to the anisotropy of the material and odd distribution of the strain it requires study of strain in the different zone. There different material and processing parameters which affect the strain pattern are considered. Present work is to study the different strain pattern and what are the different parameters which affect the strain pattern by considering different shape of the initial blank, optimization of the different material and processing parameters with the FEA simulation. The FEA simulation and experimental validation of the simulation with the flow limit curve. For reducing time required for the input parameters macro in the ANSYS parametric design language (APDL) is used.

The investigations have been carried out with the following objectives.

1. Study of different material and processing parameters that affect the deep drawing.
2. Finding the initial blank size with the line method.
3. Optimization of the initial blank by considering different shapes of initial blank.
4. Finding the optimum die radius, punch radius and clearance by FEA simulation.
5. Finding binder force with the R_{off} which gives normalize difference in stretching at the corners and side walls of the rectangular shell.
6. Numerical simulation of the process with the use of the LS-DYNA.
7. Effects of different shapes of the blank on the strain pattern.
8. Plotting the flow limit curve (FLC) for the process.
9. Experimental validation of the process with the mechanical press.

10. Comparing the FLC of FEA simulation of the process and experimental results.
11. Creation of macro with the use of ANSYS parametric design *language* (APDL) in ANSYS for the process which covers some of the input parameters of the deep drawing of rectangular aluminum cup.

1.3 Methodology.

The present study is concerned with different parameters that affects strain patterns the deep drawing process. Optimization of those parameters with the use of the R_{off} functions those cover that parameters. Determination of the initial blank size is carried out with line method. Optimization of the blank is carried out by considering different blank shapes.

As there are difference between the stretching heights at the corner and side wall in the square shell in the deep drawing process the offset value is calculated with the offset function which depends upon the central strain. Determination of the binder force is carried out with the R_{off} value.

After calculating the initial blank size and binder force numerical simulation is carried out with the ANSYS-LS DYNA software. For the FEA simulation the main concerned thing is material model, the contact algorithm and binding force. After the simulation, strain patterns are analyzed. Flow limit curve is plotted for the process because it shows the limiting Major and Minor strain and the safe region of the process.

Experimental validation of the simulation is carried out on the 20 tonnes capacity mechanical press. Flow limit curves are plotted with the grid's elongation and comparison of both experimental and simulated flow limit curve is carried out. As different material and processing parameters have considered the macro is required for the better handling of the available parameters and that is developed in ANSYS parametric design *language* (APDL).

CHAPTER 2
Literature Review

2.1 Introduction

There are many processing and material parameters which are affecting drawing process. Some of the functions are there which cover most of the material and processing parameters affecting the strain pattern and also the quality of the product. During the last decade many researchers have provided those functions which increase the efficiency of the process and reduce the undesirable features like earing and wrinkles. Some of the functions which are covering most of the material and processing parameters and also the effect of different material and processing parameters are shown. So effect of different parameters on the deep drawing and introduction to those functions are given in this review.

2.2 Effects of process variables

The process parameters that affect the success or failure of a deep-drawing operation include punch and die radii, punch to die clearance, press speed, lubrication, and type of restraint of metal flow.

2.2.1 Effect of die radii.

As the blank is struck by the punch at the start of the drawing, it is wrapped around the punch and die radii; the stress and the strain developed in the work piece are similar to those developed in bending. The force required to draw the shell at intermediate position has a minimum of three components. [1]

- The forces required for ending and unbending the metal flowing from the flange into the side wall.
- The forces required for overcoming the frictional resistance of the metal passing under the blank holder and over the die radius.
- The forces required for circumferential compression and radial stretching of the metal in flange.

So increase in the die radius reduces the work required for the deforming as punch radius has not significant affect on the process but it should be appropriate.

On the profile of the die radii flow of the material takes palace. Most of the bending and unbending takes place in that region. Die radii should be optimized for the minimization of the drawing load.

Some details on the several parameters which affect the optimal die curvature are shown below. [2]

- The effect of friction coefficient is shown in fig2.1. It is sheen that optimal die radii can be found only for very low coefficients of friction.

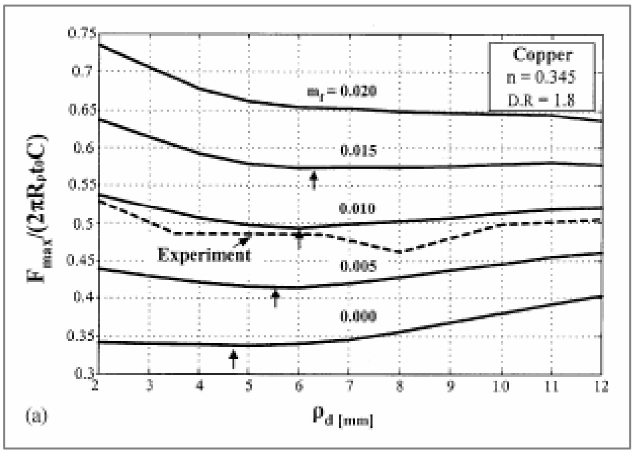

Fig: 2.1 Effect of coefficient of friction on die radii.

- The effect of strain hardening exponent is shown in fig2.2. It is apparently more useful to increase the die curvature when drawing material with relatively high strain hardening exponent.

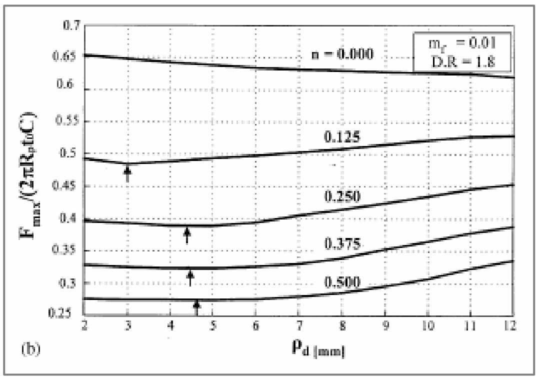

Fig: 2.2 Effect strain hardening exponents on die radii.

- The effect of drawing ratio is shown in fig2.3. Higher drawing ratio increases the optimal die radii.

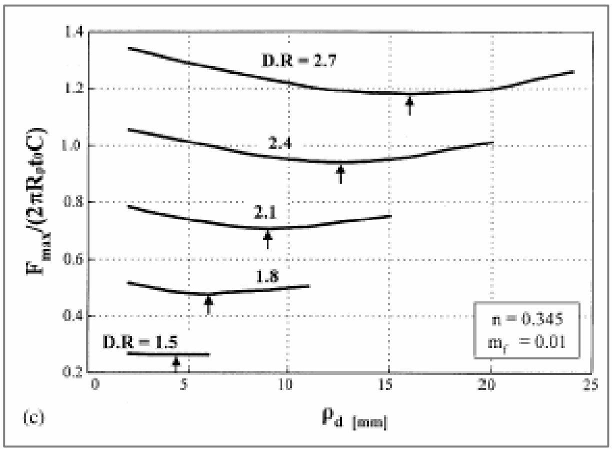

Fig: 2.3 Effect of drawing ratio on die radii.

- The effect of initial blank thickness is shown in fig2.4. The upper bound solution indicates that initial thickness has negligible effect on optimal die radii.

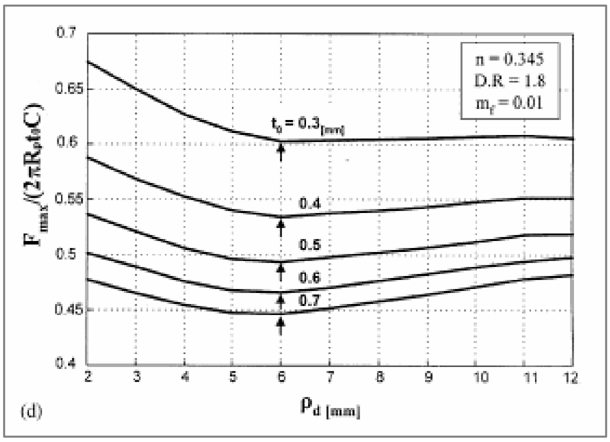

Fig: 2.4 Effect of initial blank thickness on die radii.

2.2.2 Effect of punch-to-die clearance

The selection of the punch-to-die clearance depends on the requirements of the drawn part and on the work metal. Because there is a decrease and then a gradual increase in the thickness of metal as it is drawn over the die radius, clearance per side of 7 to 15% grater than stock thickness helps prevents burnishing of the side wall and punching out of the cup bottom. Clearance between the punch and die for a rectangular shell, at the side walls and at the ends is same as in the circular cup. Radius at the corner may be as much as 50% greater than stock thickness to avoid ironing in those areas.[3]

2.2.3 Effect of blank holding force.

Even simplest drawing operation, the thickness of the work metal and die radius offers some restraint to the flow of the metal into the die. For drawing all but simplest of the shape some restraint is required for the controlling the flow of the material. [3]

Compressive forces on the metal in the area beyond the edges of the die cause the work metal to buckle. If this buckled or wrinkled metal is pulled into the die during the drawing operation, it increases the strain in the area of the punch nose to the point at which the work metal would fracture soon after the beginning of the draw. The blank holder force is used to prevent this buckling and subsequent failure. The amount of blank holding force required is one third of the drawing. [4]

Fig: 2.5 Effect of blank holding force on wrinkling

As can say that blank holding force prevent blank from the buckling and for the proper distribution of the strain, blank holding force is required otherwise problem like wrinkles can also occurs which is shown in the fig: 2.5 with and without friction.

2.2.4 Effect of the press speed.

Speed is of greater significance in drawing stainless steels and heat resistant alloys than in drawing softer, more ductile metals. Excessive press speeds have caused cracking and wall thinning in drawing these stronger, less ductile materials.[1]

2.2.5 Effect of lubrication.

When two metals are in sliding contact under pressure, as with the dies and the work metal in drawing, galling (pressure welding) the tools and work metal is likely [1]. When extreme galling will occurs, drawing force will increases and becomes unevenly distributed causing fracture of the work piece.

Selection of the lubricant is depends on the ability to prevent galling wrinkling, or tearing during the deep drawing. It is also influenced by ease of application and removal, corrosivity, and other factors.

2.3 Effects of material variables.

2.3.1 Anisotropy:

There are two types of anisotropy that must be considered; planar anisotropy, in which properties very in the plane of the sheet, and normal anisotropy, in which the properties of the materials in the thickness direction differ from those in the plane of the sheet.

Planar anisotropy causes undesirable earing of the work material during drawing [1]. Between the ears of the cup are valleys in which the materials had thickened under compressive hoop stress rather elongating under radial tensile stress. This thicker metal sometimes forces die open against blank holder pressure allowing the metal in the relatively thin areas near the ears to wrinkle.

The flange shape contours with respect to change of angle are shown in fig2.6. at different punch stroke. *Hoon hua* et.al. had carried out, that there is more material flow into the cavity at an angle 0^0 than at an angle 45^0 and 90^0 .The difference is caused by the planer isotropy of the sheet metal. Although the change in flange shape contour is not remarkable, the rolling direction on the initial blank on the deformation of the sheet metal as well as thickness strain and should be considered for the proper manufacturing. [4].

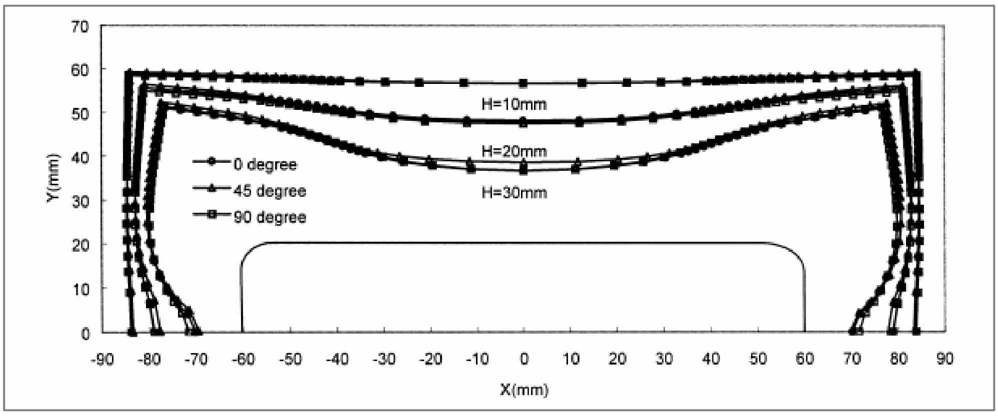

Fig: 2.6 Comparison of flange shape contours with respect to change of rolling direction in the initial blank.

Fig2.7. shows the thickness strain distribution in the deformed parts along the longer side at different punch strokes. The sheet metal becomes thinner near the punch radius and thicker near the flange region when the angle of the rolling direction to the longer side axis is 90 compare to the other two cases. [8]

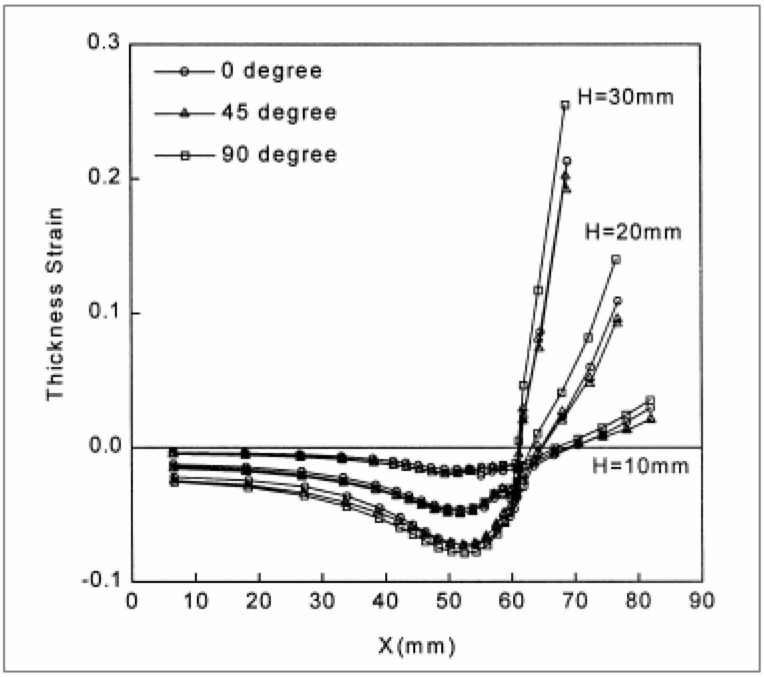

Fig: 2.7 Comparison of thickness strain distribution

2.3.2 Thickness

In deep drawing, the pressure on the dies increases proportionally to the square of the thickness. The pressure involved is concentrated on the draw radius, and increasing sheet thickness will localized wear in this area without similar effect on the other surfaces of the die [1].

Thick stock has lesser tendency towards wrinkle than thin stock. As a result, blank holder pressures used for the drawing of thick sheet be no greater, and may even be less, than those used for thinner blanks.

As deep drawing is very complicated process all the material and processing parameters has their combined effects which have to consider for the better result. Below different effect are shown.

2.4 Effect of different material and processing parameters on limiting drawing ratio

Successful forming of the sheet metal component depends on many factors and on of them is drawability. For the drawability of the material limiting drawing ratio is required. Many researchers have studied the effect of normal anisotropy, strain hardening exponent on limiting drawing ratio. The limiting drawing ratio is depends on the anisotropy value, higher the value of anisotropy value better the limiting drawing ratio. The present model considered bending and unbending around the die arc radius. Combined effect of process variables are examined based on the force lines, the type of fractured cup and thickness strain distribution. The constant fractured force and translation fracture force were defined. From the experiments following results were found:

- Influence of processing variables on limiting drawing ratio and fracture.
- Influence of processing variables on maximum drawing force and fracture force.

So from that experimental results prediction of the LDR and type of fractures are examined which depends upon the thickness distribution and force sustain-ability. The deep drawability of square cups could be explained using force lines because the sets of the lines were characterized for each of the shape factors and materials Some of the parametric studies carried out by *Rahul K. Verma* et.al. *are* shown.

Fig: 2.8 Shows the effect of coefficient of friction on the LDR. It can be seen as coefficient of friction increases the LDR decreases.

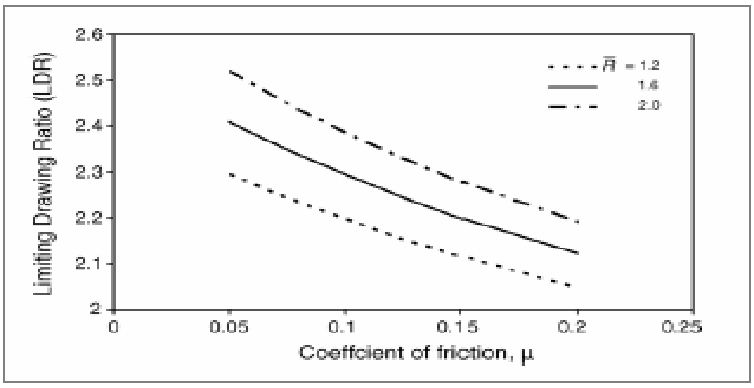

Fig: 2.8 Effect of coefficient of friction on LDR

Fig.2.9 shows effect of anisotropy coefficient on the LDR for different coefficient of friction. It is seen that there is positive relation between anisotropy coefficients value LDR. It is observed, from the slop of the curves, the effect of anisotropy value on LDR is more when friction is less.

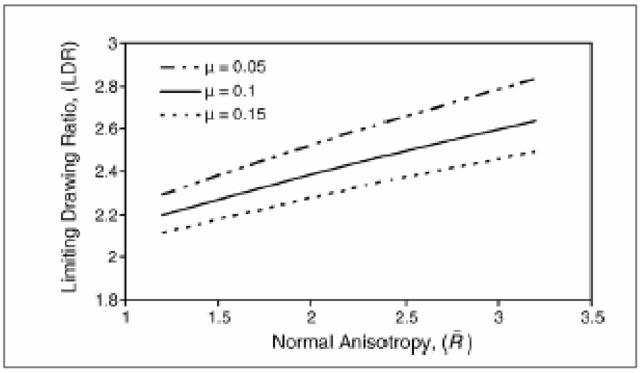

Fig: 2.9 Effect of normal anisotropy on LDR.

Fig 2.10 Shows effect of sheet metal thickness on LDR. It is clear that, with increase in sheet metal thickness, LDR increases then becomes almost constant.

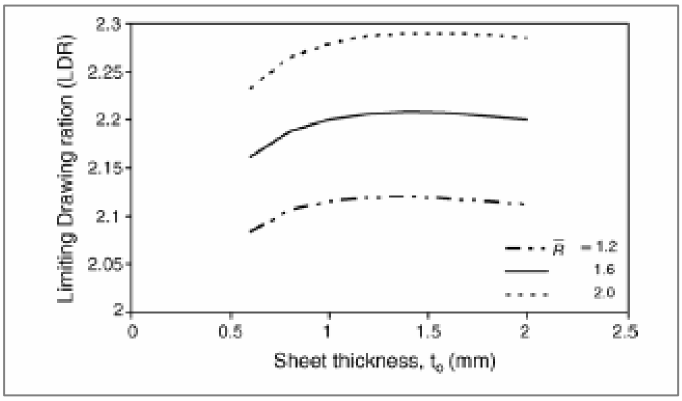

Fig: 2.10 Effect of sheet thickness on LDR.

Fig: 2.11. shows effect of strain hardening on drawability. It is clear that with increasing n LDR first decreases and then increases.

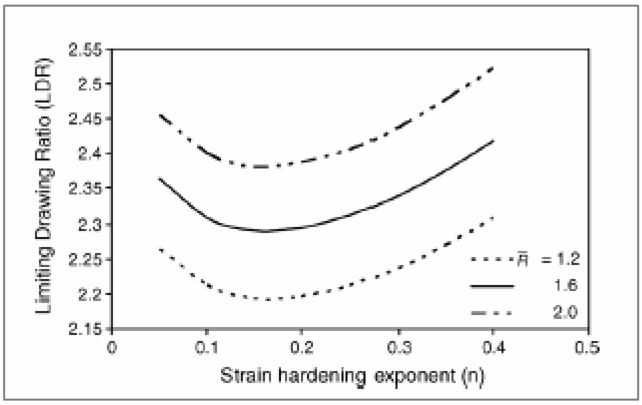

Fig: 2.11 Effect of strain hardening exponent on LDR

2.5 Effect of material properties on formability

Effect of material properties on sheet metals vary considerably, depending upon the base metal alloying element present, processing, heat treatment, gage and level of cold work. For good formability of the material it should have:

- Distribution strain uniformly.
- Reach high strain levels without necking or fracture.
- Withstand in plane compressive stresses without wrinkling.
- Withstand in plane shear stresses without fracturing.
- Retain part shape upon removal from the die.
- Retain the smooth surface and resist surface damage.

2.5.1 Strain distribution.

Three material properties determine the strain distribution in a forming operation.

1. The strain hardening coefficient.
2. The strain rate sensitivity or m value.
3. The plastic strain ratio or anisotropy factor r.

The n value is determined by the flow stress on the level of strain. Material with high n value the flow stress increases rapidly with the strain. This tends to distribute further strain to region of lower strain and flow stress.

In the region of uniform elongation the n value is defined as:

n= $d\, ln б_T / d\, ln\, ε$

Where, $б_T$ is the true stress.

Rate sensitivity m is defined as:

m= $d\, ln б_T / d\, ln\, \dot{ε}$

Where, $\dot{ε}$ is strain rate dε / dt.

The positive strain rate sensitivity indicates the flow stress is increases with the rate of deformation. This has two consequences. first higher stresses are required to form part at higher rate, second in given forming rate, the material resists further deformation in the regions that are being strained more rapidly than adjacent region. This helps to distribute the strain more uniformly. The need for higher stresses in forming operation is usually not a major consideration, but ability to distribute strain can be crucial. This is become particularly important in the post uniform elongation region where necking and high strain concentration occurs. An approximately linear relationship has been reported between m value and post uniform elongation.

High n and m values lead to good formability in stretching operation, but have little effect on drawability. In a drawing operation metal in the flange region must be drawn without causing fracture in the wall, which is beneficial, but they are also strengthening the flange and make it harder to draw in, which is detrimental.

The r value or plastic strain ratio relates to drawability and it is known as anisotropy factor. This is defined as true width strain to the true thickness strain in the uniform elongation region of a tensile test:

$$\boxed{r = \frac{\varepsilon_w}{\varepsilon_t} \frac{\ln(\frac{w}{w_o})}{\ln(\frac{t}{t_o})}}$$

The r value is measure of the ability of a material to resist thinning. In drawing, the material in the flange is stretched in one direction and compressed in the perpendicular direction. A high r value indicates a material with good drawing properties.

The r value frequently changes with the direction in the sheet. In cylindrical cup drawing operation, this variation leads to cup with a wall varies in height, a phenomenon known as earing. It is therefore common to measure the average r value or normal anisotropy, r_m and planer anisotropy ▲r.

The property of r_m is defined as $(r_o + r_{45} + r_{90})/4$. The value ▲r is defined as $(r_o - r_{45} + r_{90})/2$. it measure of the variation of the r with direction on the plane of the sheet. r_m determines the avg. depth of the deepest draw possible. The value ▲r determines the extent of earing. The combination of a high r_m value and low ▲r value provides optimum drawability.

Hot-rolled low carbon steels have r_m values ranging from 0.8 to 1; cold rolled aluminum killed steel range 1.4 to 2.0 and aluminum alloys range from 0.6 to 0.8. The theoretical maximum r value for ferrite steel is 3.0.

2.6 Combined effect of tool geometry and strain characteristic coefficient on the deep drawability

Yasyo Maramo et.al. have carried our effect of n and shape factor on the deep draw ability are described below [6].

Fractured types are both influence by n- value and corner radii of the square punch. However limiting drawing ratio is decreased under the following two conditions:

- When blank having higher n-value were drawn with square punches of small radii.
- When blank is drawn with lower n- value and with square punch having higher radii.

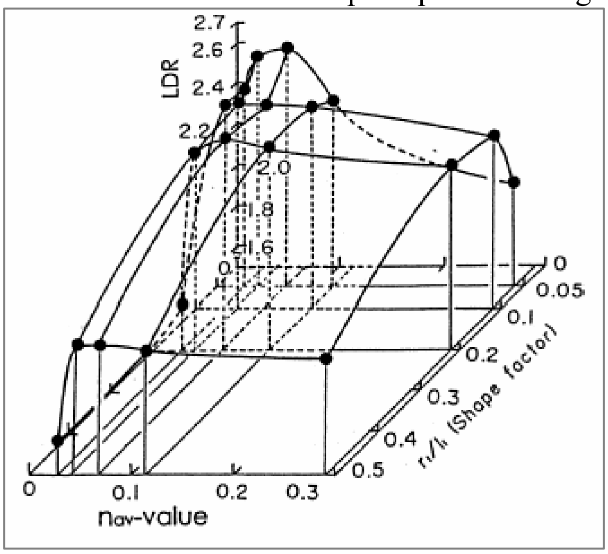

Fig:2.12 Effect of n and shape factor on LDR.

There are different types of the fractures can occur in the deep drawing like circumferential fracture, corner fracture, at the both die and punch. which depends on the thickness strain at that portion of the blank. In the fig different types of fractures are shown that can occur in the deep drawing. (fig2.13)

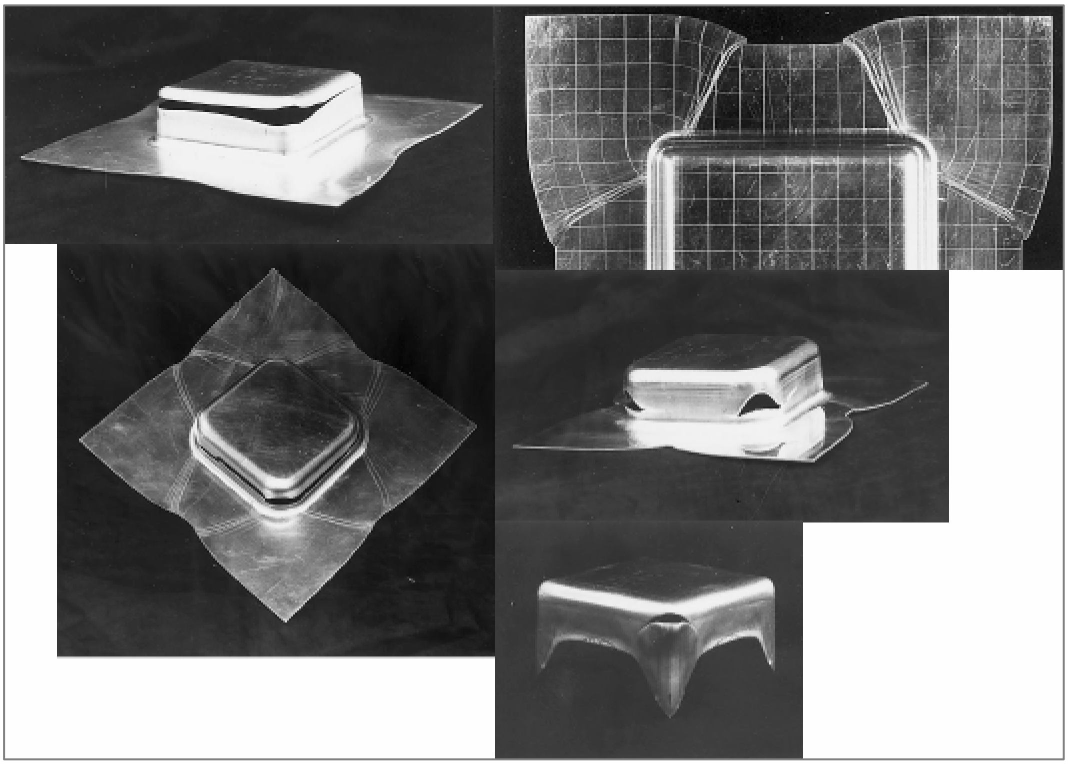

Fig: 2.13 Types of fractures.

The combined effect of strain hardening of pure aluminum sheets and tool geometry were investigated. (fig2.12)

- The influence of shape factor and n_{ag} on the fracture type.
- The slip bands occurred between the corner flange and side flange and propagated through the wall corner of the drawn cup. The occurrence of the slip bands weakened the material at the location in which slip band propagated, and induced at localized wall fracture at the large shape factor.
- The constant fracture force is the final goal for the improvement of deep drawability. The difference between constant fracture force and limiting critical force indicates the extent of the improvement in deep drawability.

Fig.2.14 (a) thickness strain distribution in the slip band region is shown. The feature of the localized fracture types can be accounted for distributions of the true thickness strain in the flange for different *n* value. Large true thickness strain is seen in the corner flange near the die cavity. It is follows that deformation resistance in the corner flange near the die corner is larger than at the side wall. Therefore tensile forces are concentrated at the punch corner and crack easily occurs at that location.

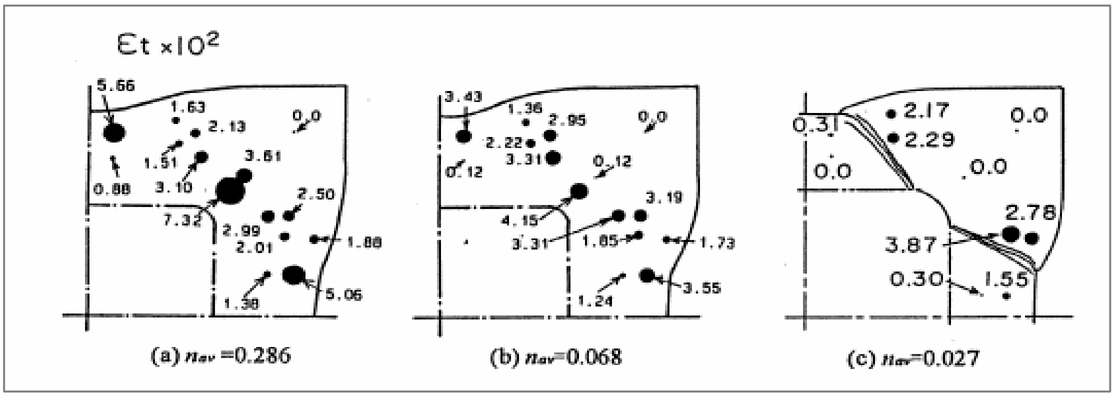

Fig2.14 Thickness strain distribution near slip band region.

Fig.2.14 (b) thickness strains in the region of drawing formation, corner near the die cavity, roughly equal to those in the straight side of the blank. It follows that the entire flange undergoes approximate uniform deformation along the circumference and drawing forces are supported circumferentially and moreover circumferential fracture tends to occur.

Fig.2.14 (c) the deformation is concentrated in the region where the slip band propagation occurs, and other body moves like rigid body. It is observed that slip bands met at the corner rim of the center of the straight side and thickness region in the corner region is remarkably increased.

2.7 Effect of different parameters on Strain distribution in deep drawing.

P.P Date and S.G. Desai had carried out 2D analysis of the deep drawing process and the parameters that affecting the thickness strain were combined into the functions called constraint factor and strain non uniformity index [7].

When a flat sheet is drawn into a product, ideally, a uniform strain distribution is desired. However, non uniformity in strain distribution is generated by the product geometry, tool sheet contact conditions and materials properties. Non uniformity in the thickness reduces the usable ductility and leads to early failure. since individual effects of the above mention factors and their combination is not easily quantifiable and often not deterministic, the combined consequence of these on these on the geometry, materials and process parameters on the variation of the constraint factors is defined as strain non- uniformity index. The quantification of strain distribution is carried out by defining parameters namely constraint factor (CF) and strain non uniformity index (SNI). The behavior of SNI and constraint factors indicates that R value and drawing ratio are most significant variables determining uniformity of strain distribution. In case of failure strain non uniformity index is very high and constraint factor is found to approach zero.

- Strain non uniformity index and constraint factor gives information about the non uniformity induced in the component at a particular instant.
- These quantities can be used for process control as decision making tool by process designer.

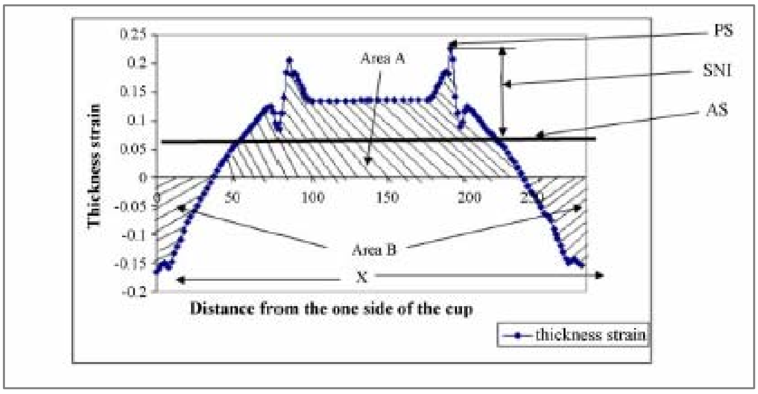

Fig: 2.15 Thickness strain distribution.

Fig.2.15 shown which indicates sharp change in the thickness strain which can be calculated by the strain non uniformity index (SNI) and constraint factors

2.8 Determination of R_{off} value and its effects

Hong yao and Jian cao had developed algorithm to find out d R_{off} which is depends upon the central strain [8]. They had developed the function of R_{off} and the rapid determination of the blank holding force with the 2D analysis and analytically. Below some of the important points are covered.

In the deep drawing of the square cup there is difference in the stretching height at the corners and at the sidewalls. Die to this difference amount of material flowing in to the die cavity is different. So for getting maximum height it is necessary to add that offset value for the blank. In this research they have provided the analytical model for the square cup considering the curve beam and then that value of the stretch height is compared with the 3d simulation height for getting thee R_{off} value.

2.8.1 Tooling geometry

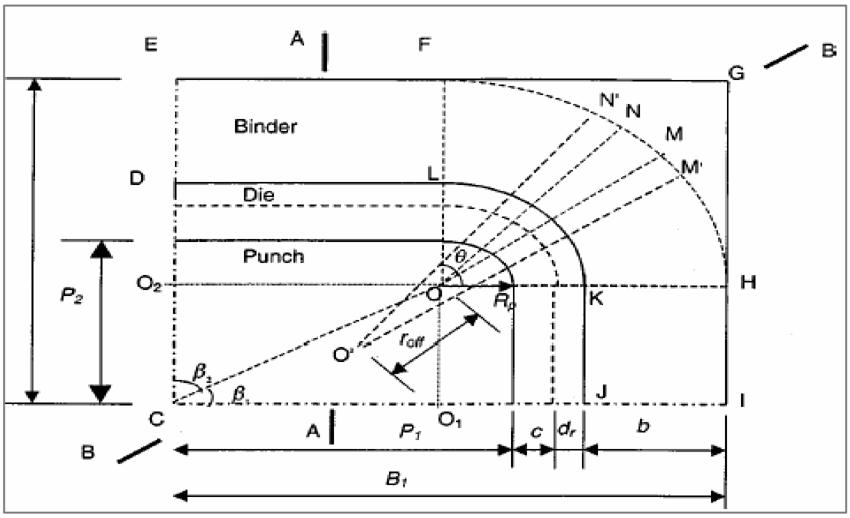

Fig: 2.16 Tooling geometry

In the above fig.2.16 the geometry of the tools are shown. As corner part is *OFGH* and side wall part *OO_2EF* and *OO_1HI* is shown. Also the center offset is shown due to which extra material is to be consider. *CE* and *CI* are the plain strain section lines, where deformation is assumed to be plain strain condition.

2.8.2 2D model with center offset.

The conventional method treats OFGH as an axisymmetric model and OMN as 2d simplified axisymmetric model. As a result model does not take into account the material stretched into the corner section from under the punch and material flowing toward the corner from the straight sides as the punch advances. Consequently, it provides conservative result, meaning that corners can actually form deeper than that predicted. So for that the offset value is used for the 2d model for the proper restraining force.

2.8.3 Determination of Stretch heights.

In the fig2.17 different stretch height at the corner and at the side wall are shown. The stretch height shows how the material is pulled out from underneath of the punch and they are directly related to the final forming height. Difference in the height is calculated from this equation.

$$D_C-D_S=0.4(1-COS\Theta)^{1/2}D_S \ldots\ldots\ldots\ldots\ldots\ldots\ldots\ldots\ldots\ldots\ldots\ldots(1)$$

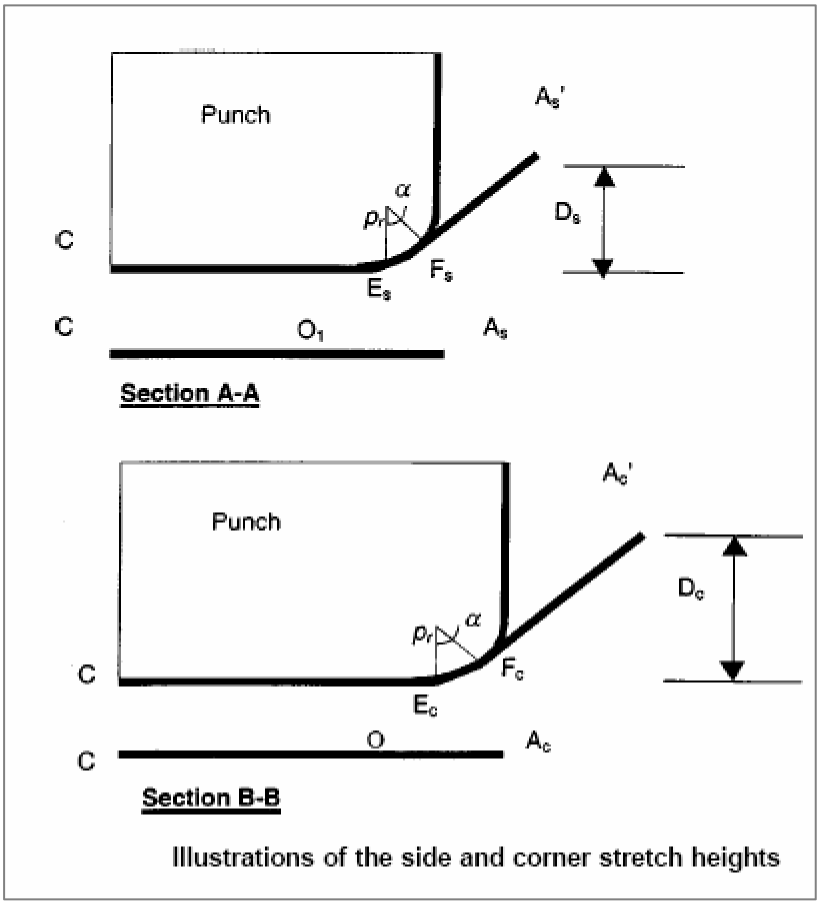

Fig: 2.17 Illustration of side and corner stretching heights

2.8.4 Finding the offset value for the base model.

The right offset is obtained when failure height predicted by the 2D model is equal to 3D model. Obviously, offset depends upon the tooling geometry and processing parameters such as material properties and binder force etc. For the value analytical model is developed. Stretch height difference can be calculated from the:

$$Dc\text{-}Ds = \frac{0.4Ds}{\sin\alpha} - 0.4\varepsilon c(Po - Rpo) \quad \ldots\ldots\ldots\ldots\ldots\ldots\ldots\ldots(2)$$

The center strain is considered as important design specification in the stamping part as these values directly relates to the strength of the panel. When designing the central strain section, the 2D section analysis model is used to finding certain restraining forces.

Restraining force at the corner and at the side walls is calculated from the:

$$Fs = \frac{A_1 F_b}{(A_1 + A_2 + A_3)(P_1 - R_p)\tan\beta_1} \quad \ldots\ldots\ldots\ldots\ldots(3)$$

$$Fc = \frac{A_3 F_b}{(A_1 + A_2 + A_3)(R_p + C + dr)\theta}$$

The difference of restraining stress б, at the draw wall area can be defined as;

$$б = \frac{2\varpi(Fc - Fs)e^{\mu\alpha}}{t} \quad \ldots\ldots\ldots\ldots\ldots\ldots\ldots\ldots\ldots\ldots(4)$$

The empirical relation of the central strain and R_{off} value and blank holding force was earlier found by *Hong Yao, Brad L. Kinsey, Jian Cao* [14].

Empirical relation between the R_{off} is given below.

$$R_{off} = \frac{0.358 FLD^{2.1286} k^{1.3853}}{\varepsilon_c^{1.4106} p^{4.2318} y_p^{0.4334} c_p^{0.6411} \mu^{1.0643}}$$

For the binder force:

$$F_b^{\,e} = \frac{Fb(A_2 + A_4)(R_{off} + r_s)\theta}{2\pi(A_1 + A_2 + A_3 + A_4) r_s}$$

2.8.5 Analytical model used to calculate the Roff value.

Schematic diagram (fig.2.18) shows the model to calculate the center offset. The arc is subjected to uniform distributed force which is equal to the difference of restraining force. Assuming deformation as elastic the solution of the deflection can be approximated as.

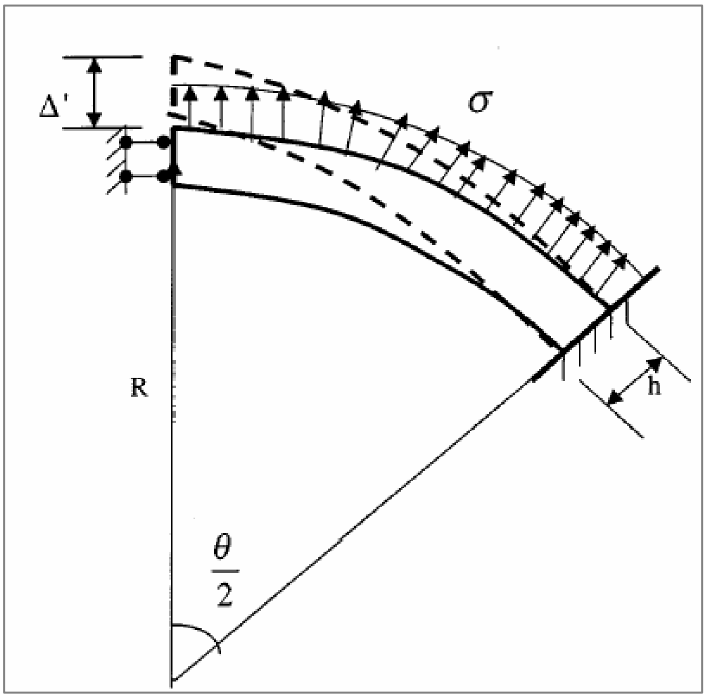

Fig: 2.18 Analytical model to determine offset value.

$$\Delta' = \frac{\gamma \sigma R^2 t_o}{Eht} \quad \ldots\ldots\ldots\ldots\ldots\ldots\ldots\ldots\ldots\ldots\ldots\ldots..(5)$$

The offset in the 2d axisymmetric can be calculated by:

$$r_{off} = \left[\left(\frac{Eht}{\gamma to\sigma} \Delta \right)^{1/2} - h/2 - Rpo + \Pr o(1 - \sin\alpha) \right] \frac{1}{(a_1 \varepsilon c + a_2)^n} \quad ....(6)$$

2.9 Different yield criteria used for the deep drawing.

2.9.1 Hill's criteria

L. Wang and T.C. Lee had carried out effect of different yield criteria on steel and aluminum alloys. They had suggested which, criteria is better for the different material. [9]

The increasing application of numerical simulation in the field of metal forming is helped to solve problem in very less period of time. Accurate simulation results are vital for die and product design. He proposed flow limit curve (FLC) which is used to evaluating necking risk, differs a lot when different yield criteria are used. *Yield criteria Hill 90* and *Hill 93* varies little and describes the accurate result for both mild steel and aluminum very well. Yield curve based on yield criteria *Hill 48* underestimated in all the region of FLC compared to the other two criteria. The simulation result with *Hill 90* is best suited for both mild steel and aluminum.

Fig.2.19 yield curves of SPCC (JISG3141) calculated by *Hill 90* and *Hill 93* very little. It is critical to choose the limit criteria. It is general thinking that Hill 48 criteria is best suited for the material like mild steel and stain less steel. The *Hill 93* and *Hill 90* are over lapping and match with the experiment results.

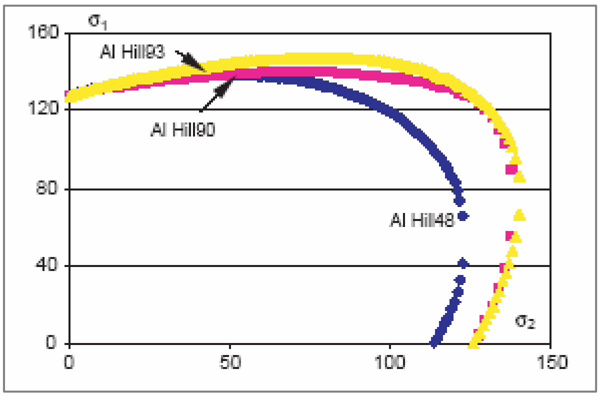

Fig: 2.19 Al6xxx yield curves calculated for three yield criteria.

Predicted limit strain is shown in fig.2.20 for the different yield criteria. The swift model and hill model are employed to calculate the limit strain located in the right and left side of the FLD respectively. For the SPCC (JISG3141) the predicted values are almost coincident with the experimental ones in the left side and are much lower than the actual calculated value in the right side of the FLD in *Hill 93*, *Hill 48* and followed by *Hill 90*. For the aluminum, theoretical value displays string consistency with the experimental value on the both the side of the FLD. In particular, calculated limit strain with the *swift* model based on *Hill 90* yield criteria coincides most with the actual v

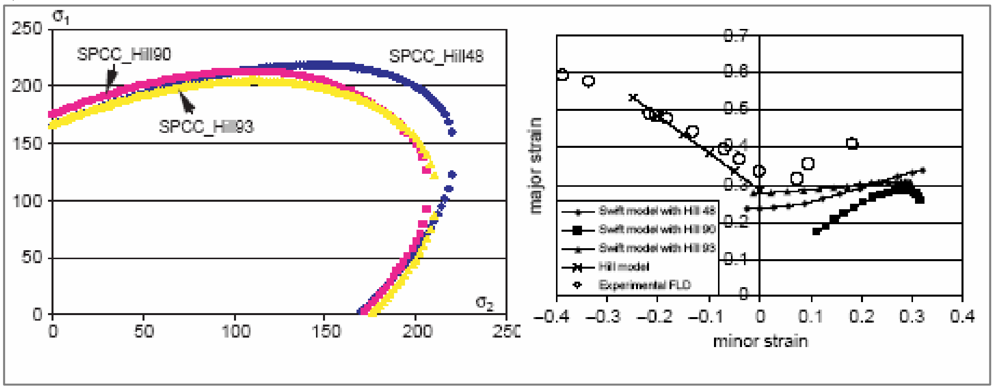

Fig: 2.20 Yield curve and calculate limit strain for different yield criteria. (SPCC)

The simulation results are shown in the fig.2.21 when adopting *Hill 48* and *Hill 90* respectively. The shapes of the product with different yield criteria look similar to each other. However, major strain differs a great deal in both the punch nose and the top areas. The simulation results with the *Hill 90* criteria are more consistent with the experimental results than *Hill 48*.

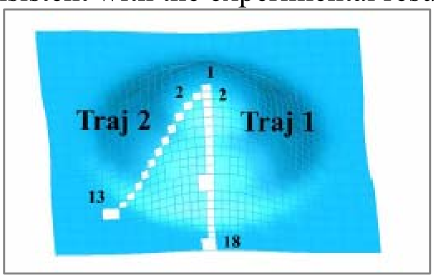

Fig: 2.21 Chosen elements and simulated product shape.

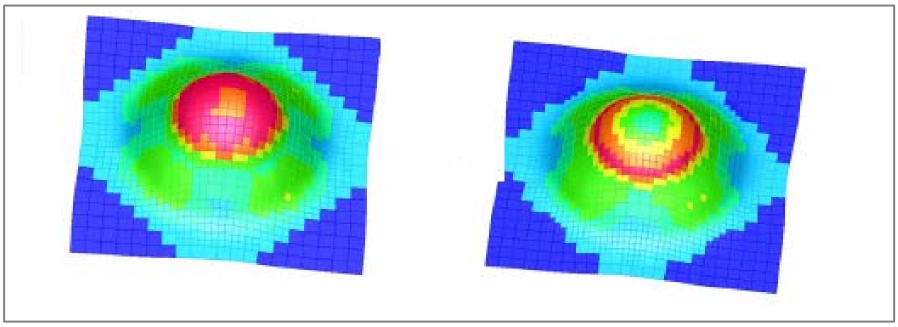

Fig: 2.22 Major strain distribution of Al6xxx with Hill 48 and Hill 90 yield criteria.

The strain values of the elements located in the trajectories 1 and 2 and the experimental results are compared with each other which are shown in the fig.2.23 and 2.24.Except few elements at the end of the trajectories, strain condition of the rest of the elements varies great deal with *Hill 48* and *Hill 90*. The strain path calculated with *Hill 90* is more consistent with the experiment one.

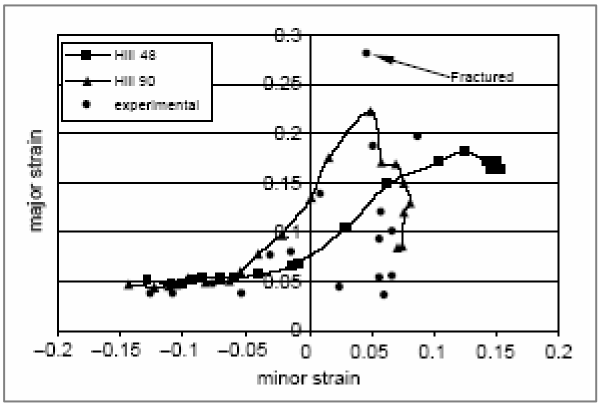

Fig: 2.23 Strain value of trajectory 1 calculated with Hill 48, Hill 90 and experimental data.

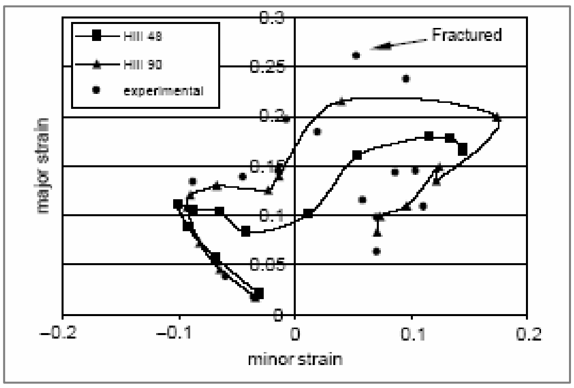

Fig: 2.24: Strain value of trajectory 2 calculated with Hill 48, Hill 90 and experimental results.

From the above results it can be concluded that *Hill 90* is best sited for the aluminum.

Another yield criteria which is also used for the deep drawing of the aluminum is the Brlat' yield criteria and which is best when defects like earing is concern.

2.9.2 Barlat's yield criteria

J.W.Yoos, F.barlat, R.E.Dick, and S.Choudhry had suggested that, the anisotropy of the sheet metal during the sheet metal forming is combination if the initial anisotropy due to its previous history of thermo mechanical processing and to the plastic deformation during the plastic deep drawing operation [10]. The former leads to symmetry with the orthotropic character while the letter called deformation induced anisotropy, can destroy this symmetry when principal material symmetry and deformation are not superimposed Barlat et.al. (2004) suggested new anisotropy model which takes into account more than four ears. The yield function requires the experiment input data every 15 degree. Thus it can capture the detailed distribution of r-value and yield stress anisotropies. Yield function is:

$$
\begin{aligned}
\phi(\tilde{\mathbf{S}}', \tilde{\mathbf{S}}'') = {} & \left|\tilde{S}_1' - \tilde{S}_1''\right|^a + \left|\tilde{S}_1' - \tilde{S}_2''\right|^a + \left|\tilde{S}_1' - \tilde{S}_3''\right|^a + \\
& \left|\tilde{S}_2' - \tilde{S}_1''\right|^a + \left|\tilde{S}_2' - \tilde{S}_2''\right|^a + \left|\tilde{S}_2' - \tilde{S}_3''\right|^a + \\
& \left|\tilde{S}_3' - \tilde{S}_1''\right|^a + \left|\tilde{S}_3' - \tilde{S}_2''\right|^a + \left|\tilde{S}_3' - \tilde{S}_3''\right|^a = 4\bar{\sigma}^a
\end{aligned}
$$

Fig.2.25 Shows yield surface of both curves predicted with yield functions and determined experimentally.

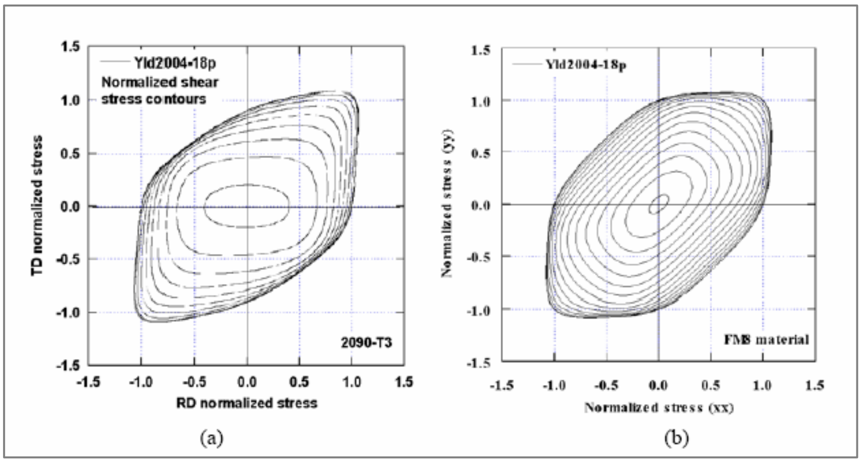

Fig: 2.25 Yield surface shape (a) AL2090-T3, (b) FM8

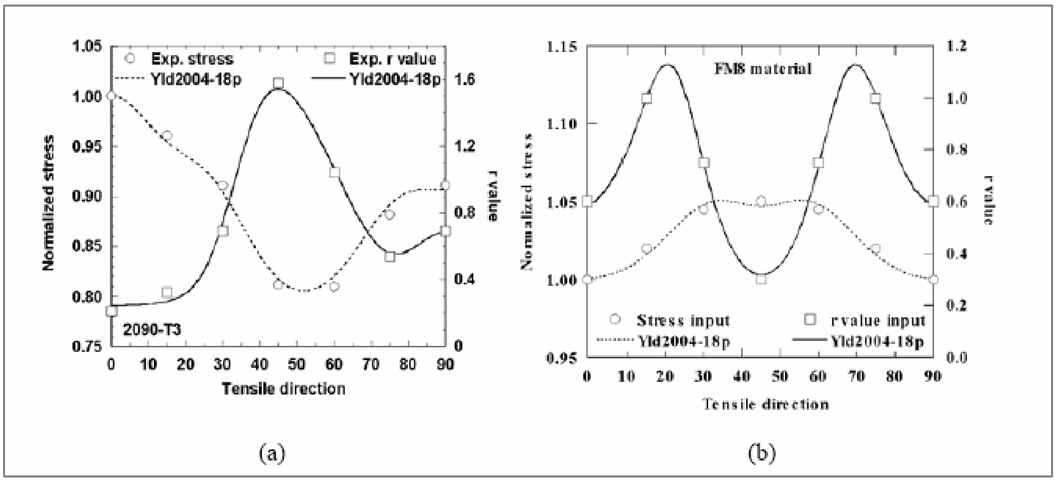

Fig: 2.26 Normalized yield stress r-plot: (a) AL2090-T3, (b) FM8

Fig.2.27 shows deformation of completely drawn cups of the aluminum alloys sheet Al 2090T3 which is generally used for aerospace applications and exhibits severe anisotropy. It is observed that AL2090-T3 material shows six ears and material FM8 shows eight ears. It is directly related to r-value distribution. The prediction of earing profile is the unique capability of the Barlat's yield function.

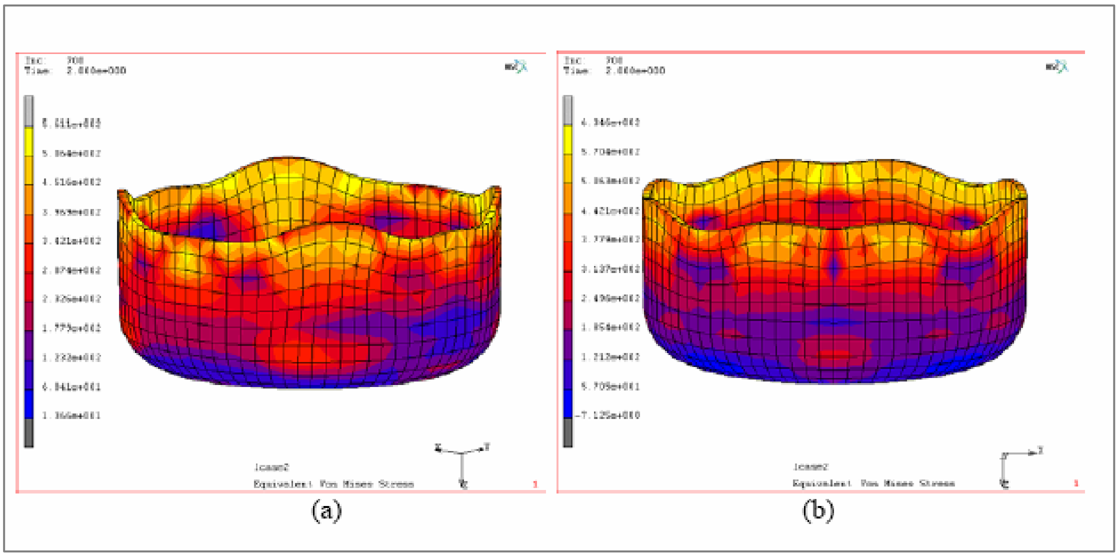

Fig: 2.27 Deformed configuration of completely drawn cup using Barlat's model. (a)AL2090-T3, (b) FM8

Fig.2.28 shows the predicted and the measured cup height profiles and compared for AL 2090 T3 sheet. For orthotropic material, the cup height profile between 0^0 and 90^0 should be the mirror image of the cup height profile between 90^0 and 180^0 with 90^0 axis. This plot show that earing profile obtained from the present theory is in very good agreement with the measured profile.

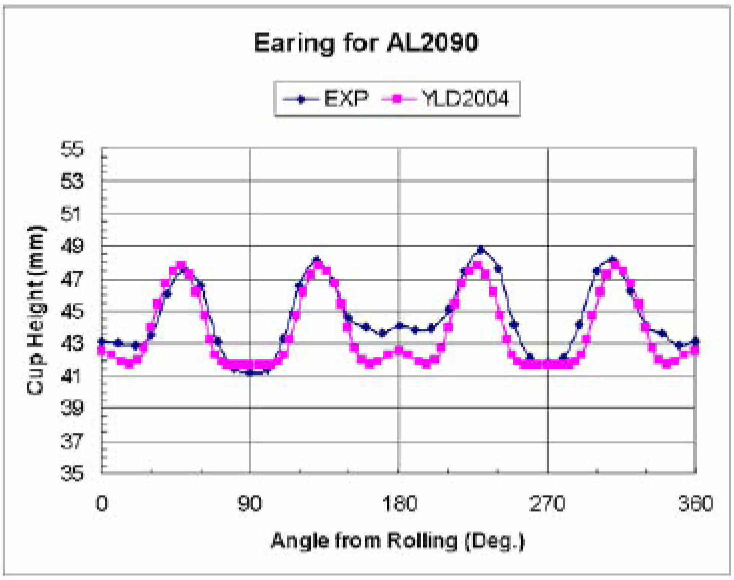

Fig: 2.28 Comparison earing profile for AL 2090 T3.

2.10 Selection of process variables for the deep drawing

Equipments, tools and techniques used for deep drawing aluminum and aluminum alloys are similar to those used for other metals. In section, those aspects of deep drawing which are specific to aluminum alloys, and is restricted to procedures using a rigid punch and die.

2.10.1 Equipment.

Punch presses are used for nearly all deep drawing process, press breaks are used for experimental or very short runs. Presses used for steel are also suitable for aluminum.

Presses speed are ordinarily higher then they are for steel. For mild draws single action press are usually operated at 27 to 43 m/min. Double action presses are operated at 12 to 3 m/min for mild draws, and at less than 15m/min for deeper draws with low and medium-strength alloys. Drawing speed on double action presses are about 6 to 12 m/ min with higher strength alloys. [1]

2.10.2 Tool design

Tools for deep drawing have the same general construction as those used with steel, but there are some significant differences. Aluminum stock must be allowed to flow without undue restraint or excessive stretching. The original thickness of the metal is change very little: These differ from the deep drawing of stainless steel and brass sheet: each of which may be reduced by as much as 25% in thickness in single draw.

Clearance between Punch and die are usually equal to metal thickness plus about 10% per side for drawing alloys of low or inter mediate strength. An additional 5 to 10% clearance may be needed for the higher-strength alloys and harder tempers.

With circular shell, metal thickening occurs with each draw, there for clearance is usually increased with each successive draws. The restriction imposed on the drawing of rectangular shells by metal flow at the corner make equal clearances for each draw satisfactory. The final operation with tapered or rectangular shells serves primarily to straighten walls, sharpen radii, and size the part accurately. So clearance for these operations is equal to thickness of the stock.

Excessive clearance may result in wrinkling of sidewalls of the drawn shell. Insufficient clearance burnishes the sidewalls and increases the force required for the drawing.

1. Radii on tools

Tools used for drawing aluminum alloys are ordinary provided with draw radii equal to four to eight times the stock thickness. A punch nose radius is some times as larger as ten ties the stock thickness.

A die radius that is too large may lead to wrinkling. a punch nose radius that is too sharp increases the probability of fracture or residual circular shock lines which can only removed by polishing.

Nonetheless, failure by fracture can sometimes be eliminated by increasing the die radius, or by making the drawing edge an elliptical form in stead of circular arc.

2. Surface finish on tool.

Draw dies and punches should have surface finish of 0.4 or less for most application. A finish of 0.08 to 0.1 is often specified on high production tooling for drawing light-gage or percolated stock.

Lubricants for deep drawing aluminum alloys must allow the blank to slip readily and uniformly between blank holder and die, and must prevent stretching and galling while this movement takes place.

The drawing compounds can be applied only to the areas that will be subjected to a significant amount of cold working, unless local application interferes with the requirements of high speed operation. Uniformity of application is critical, specially to enable the maintenance of correct blank holding pressure around the periphery of the die.

2.10.3 Drawing limits.

The reduction in diameter that is possible in single operation with aluminum alloys is about same as that obtainable with drawing quality-steel. For deep drawing cylindrical shell, reduction in diameter of about 40% for first draw, 20% for second draw, 15% for third and subsequent draws can be obtained with good practice. The part can completely formed without intermediate annealing. Four or successive draw can be obtained with proper die design and lubrication, on such alloys such as 1100, 3003, and 5005. The amount of reduction decreases in successive draws because of loss in workability due to strain hardening. The total depth of raw obtainable without intermediate annealing exceeds that obtainable from steel copper, brass, or other common materials. [1]

The rate of strain hardening is greatest for the high strength alloys and least for low strength alloys. The major portion of the change is accomplished in first draw. The rate of strain hardening is more rapid with high strength alloys.

Blank development is of particular importance in deep drawing of large rectangular and irregular shapes. Excessive stock at the corner must be avoided, because it hinders the uniform flow of metal under the blank holder and thus leads to wrinkle and fracture.

With suitable tooling and careful blank development, large regular and irregular shapes can often be produced economically in large quantities by deep drawing. Smaller quantities are made in sections with an expensive tooling and then assembled by welding.

2.11 Introduction of the forming limit diagram

Each type of steel, aluminum, brass r other sheet metal can be deformed up to certain level before local thinning (necking) and fracture occur. This level depends principally on the combination of the strains are imposed, that is the ratio of major and minor strain. The lowest level occurs at or near the plane strain condition. That is when the minor strain is zero. [1]

This information was first represented graphically as the forming limit diagram. Which is a graph of the major strain at the onset of necking for the all value of the minor strain that can be realized the diagram is used in combination with strain measurements usually obtained with the circular grid, to determine how close to failure a forming operation is or whether a particular failure is due to the inferior work material or to a poor die condition.

The shape of the curve for aluminum alloys, brass and other materials differ according to the alloying elements. The position of the curve also varies with the increase in thickness, n value, m value but they are different than the steel.

The forming limit diagram is also dependant on the strain path. The standard diagram is based on the approximately uniform strain path. Diagram generalized by uniaxial straining or the reverse, defers considerably from the standard diagram. Therefore effects of strain path also take into account when using diagram to analyze forming problem. Below in the fig. general forming limit diagram is shown. [12]

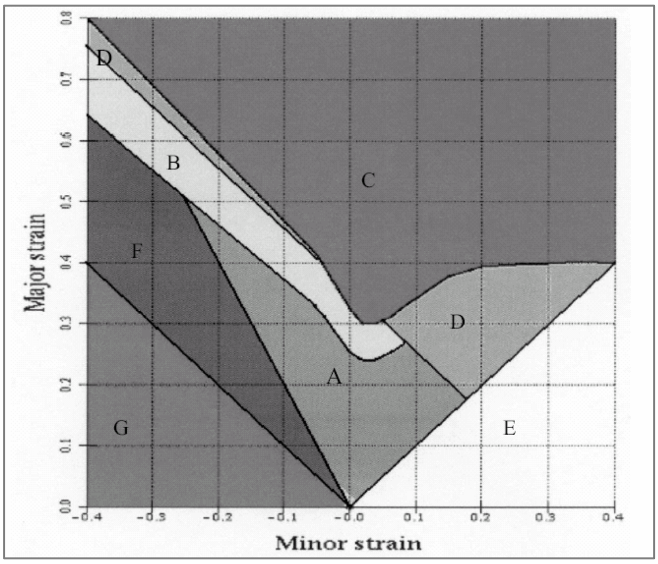

Fig 2.29 General flow limit diagram

A=appropriate use of forming ability if the material.

B=Danger of rupture or cracking.

C= The material has cracked.

D= Sever thinning.

E= In sufficient plastic strain, risk of spring back.

F=Tendency to wrinkling.

G= Fully developed wrinkles.

2.12 Determination of forming limit diagram

Forming limit diagrams indicates the limiting strains that sheet metals can sustain over a range of major to minor strain ratios. Two main types of laboratory test are used to determine these limiting strains. The first type of test involves stretching test specimens over a punch or by means of hydraulic pressure- for example, the hemispherical punch method. This produces some out of plane deformation and when a punch is used, surface friction effects. Second test produces only in plane deformation and does not involved any contact with the sample within the gage length.

The strains are measured in and around visible necking and fracture. The forming limit curve is drawn above the strain measured outside the necked regions and below those measured in necked and fractured region

In plane deformation of the forming limit diagram can be achieved by using the uniaxial tensile test, rectangular sheet tension test, or *Marciniak* biaxial stretching test with elliptical and circular punches. The forming limit curve can be determined over the full range of the strain ratio, without considering any out of plane deformation.

2.12.1 Circular grid analysis.

Circular grid analysis is useful technique ensuring that the die is adequately prepared for production and diagnosing the causes of necking and splitting failures. The forming limit diagram for the type and gage of work mater selected must be obtained. Array of small diameter (2.5mm, 0.1 in.) even spaced circles are printed or etched in several blanks n several critical strain region. Critical strain region of the parts are identified by visual observation of necking and splitting, or by previous experiment of similar part. The local strains are calculated and plotted on to the limiting diagram. [1]

If maxing strain is measured close or above the limiting strain problem with the tooling, lubrication, blank size or positioning, or press variables are indicated, whether or not actual splitting occurs.

If major strains are measured below the limiting strain a necking or splitting occurs, the batch work material is sub standard. The material used in the die layout must have typical slightly lower, forming properties than production material. The use of superior material may indicate an adequate safety margin that will disappear when more typical or lower formability material used.

Many types of circle grid pattern have been used, such as square array of contacting or closely spaced, non contacting and over lapping. The contacting and over lapping circle provide improved coverage, but more difficult to measure manually.

With closely spaced circles it is possible to measure strain gradients accurately, provided that circles are not to be small for accurate measurement. Circle with 2mm size found to be a good size. Both open and solid circles have been used. The circle grids can be applied to the blanks by printing or photographic technique or electrochemical etching. Now these days laser marking is also used.

2.12.2 Measuring circle from the deformed circles.

Deformed circles can be measured manually by means of dividers and rulers, graduated transparent tapes or low power microscope with graduated stage. Automatic systems, known as grid circle analyzer and digital laser analyzer have been also developed for measuring dimensions of circles and calculating minor and major strains.[1]

The region of high curvature, the most accurate method of measurement is use of transparent tape because it follows the contour of the part and measures the arc length. The tapes have diverging lines to give direct readings of strain.

2.12.3 Implementation of forming limit diagram in FEM simulation

In recent years application of sheet metal parts in production has becomes more and more important. Knowledge of the formability of the sheet metal is critical for the success of the sheet forming operation.

Implementation of the forming limit diagrams in FEA simulation.

M.Samuel has suggested that FEM simulation will be able to predict the forming load, the geometric changes of the deformed sheet, the distribution of the stress and strain and conditions. The FLSD is independent of the deformation and more useful than the classical forming limit diagram. [12]

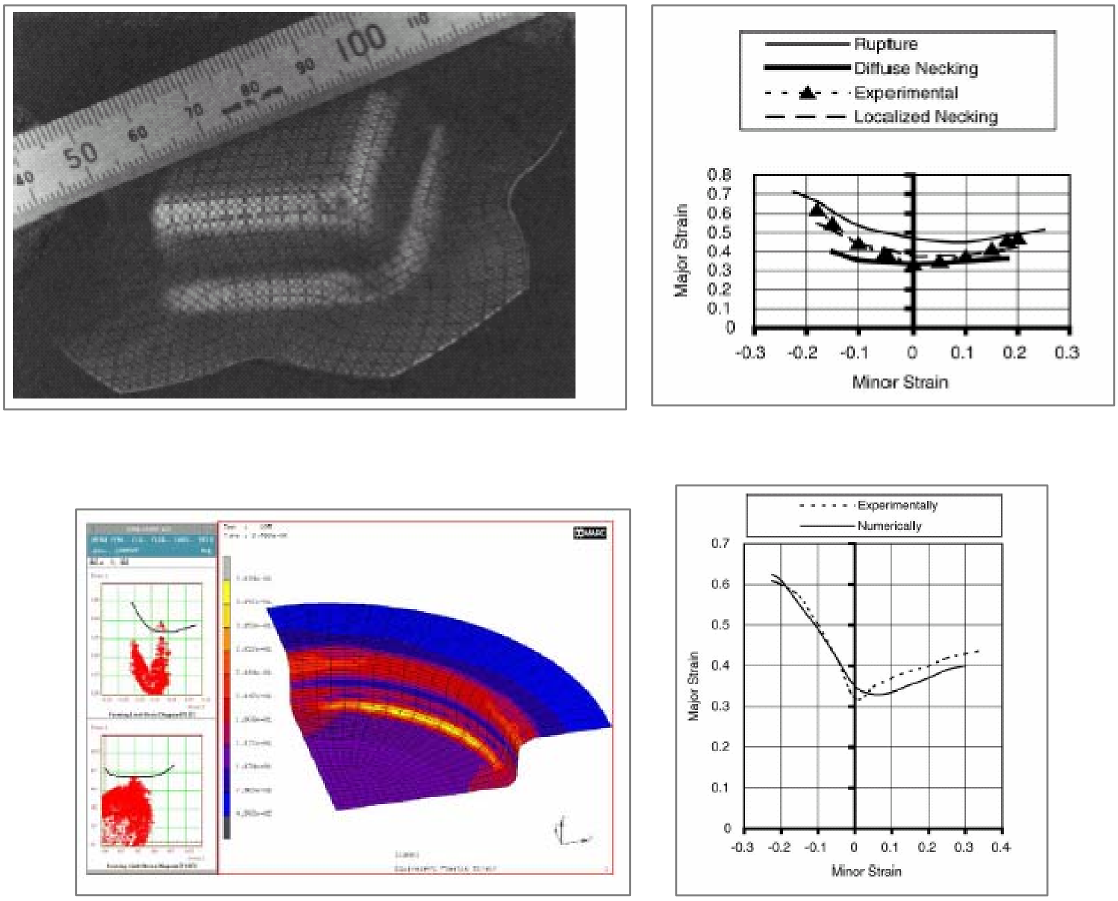

Fig: 2.30 FEM simulation of square cup

In the above fig FEM simulation of the square cup with the FLD and FLDS is shown. Though FLD method is proven to be useful tool in the analysis of forming severity, it has been to be valid only for cases of proportional loading, where the ratio between the principal stresses remain constant through out the forming process. This condition is sometimes falsely equated to the condition of proportional straining, where the ratio of the principal plastic strain remain constant. Since later ratio is observed by both measurement and FEM prediction to be nearly constant during most first draw operation and this process is considered most critical with respect to formability. The path dependent limitation of the FLD is not considered.

In this chapter earlier work on the deep drawing process are shown. There are many processing and material parameters, which are affecting the process. Different parameters that affecting formability limiting drawing ratio, thickness strain and R_{off} is considered. So, main areas of concerned are the proper selection of those parameters for the successful manufacturing of the part.

In the next chapter determination of the initial blank size with the line method and drawing force is carried out. Also, determination of the R_{off} value for the binder force is carried out.

CHAPTER 3

Determination of Initial blank size, drawing force and R_{off} value.

3.1 Introduction

To start with the process of obtaining flow limit curve and strain pattern initial shape or blank size is required for the FEA analysis to study the deformation process. A method called line analysis technique has been proposed to determine initial blank geometry. The material here considered is *Aluminum 1100*

This technique is employed to decide upon the initial blank size used for first step of the analysis. An ideal case is considered in this technique that the whole blank material is drawn into the cup shape without any stretching and thickening effect.

3.2 Blank development

Centers of the corner radii *Rc* of blank lie on the intersections of the center lines of radius '*r*' on the bottom of the box. Corner radius *Rc* can be found from the following equations:

$$Rc = (R^2 + 2Rh - 1.141\, R\, r)^{1/2} \qquad \text{……………………………………(3.1)}$$

R = Corner radius joining vertical sides of the box.

r = Corner radius joining horizontal bottom to vertical sides of the box.

h = height of the box.

For finding the shape of the corners, arc is drawn with radius *Rc* from centers *A, B, C, D*. Then draw lines representing top edges of the box at distance *(h + Π r/2)* from the lines passing through *A, B, C, D*. Draw the bending radius such a way that it is tangential to the lines representing top edges and the corner radius as drawn earlier. The corner radius and the blending radius together constitute the corner profile of the blank.

3.3 Determination of Corner radius and box height.

Fig shows the recommended radii between the sides, and bottom and sides. Corner radius *R* between the sides should preferably be more than one- tenth of the length *L* of the box. The radius joining the bottom to the sides' *r* generally rages from three to eight times the blank thickness *T*. The height of the box *h* depends upon the corner radius *R* between the sides.

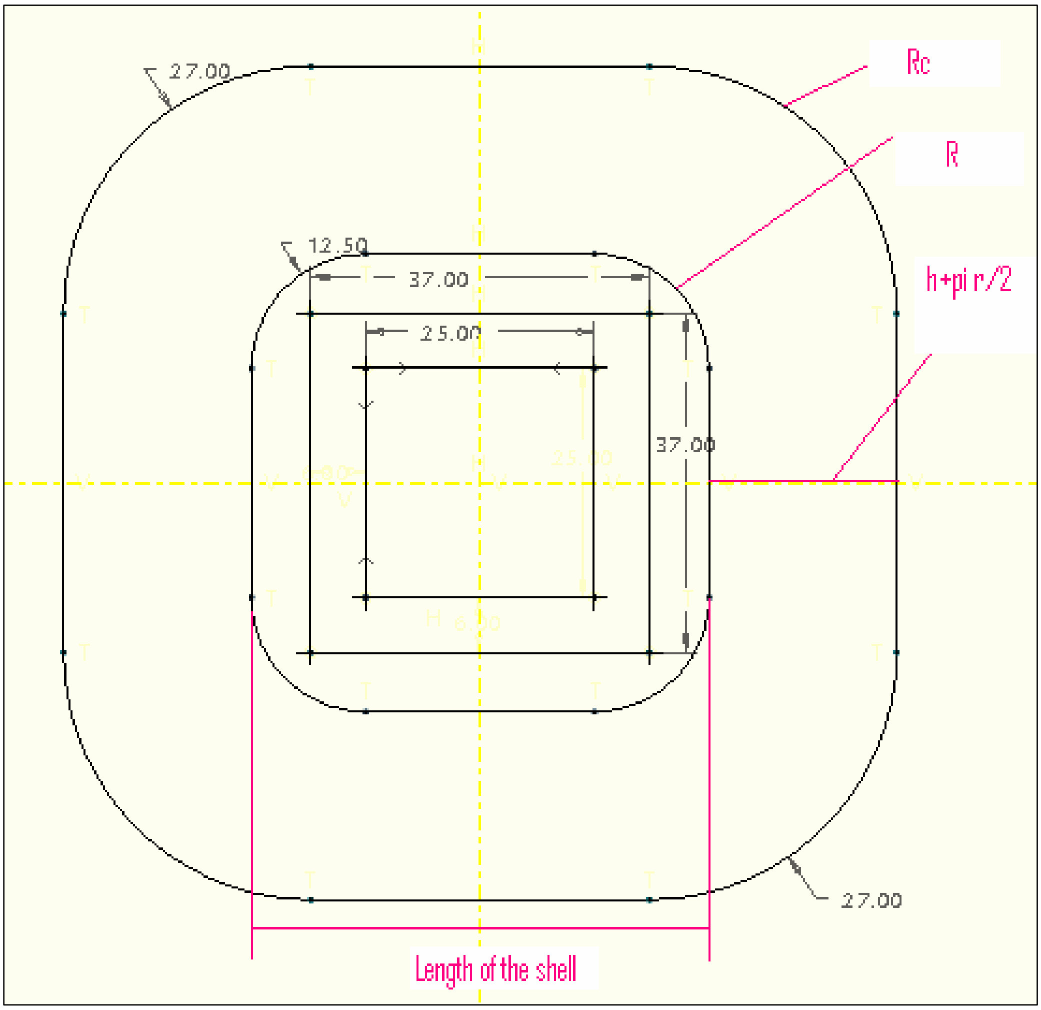

Fig: 3.1 Geometry of the initial blank size.

Limitation on the *h* and *R* values

h <= 12R if R <= 6

h <= 6R if R 12-25

3.4 Determination of Drawing force.

The force required for square drawing can be found from the following equation. Here 30% blank holding force is considered for as the initial value.

$Vdr = ft\ T\ (2\Pi\ R\ C + 0.25\ L)$..(3.2)

Where,

ft = Ultimate tensile strength.

T = Thickness of the blank.

R = Corner radius between the sides.

L = length of the box.

C = Constant depending on the ratio h/R.

Table 3.1: Value of the *C* from *h/R* ratio.

h/R	2	6
C	0.5	2.0

3.5 Input variables for the Determination of drawing force.

Experiment is carried out with the mechanical press of the 20 tonnes capacity. There is minor difference between the deep drawing shallow drawings. If the height of the cup is more than one half of one of its side then it is called is deep drawing and if it is less than that it is called as shallow drawing. As in the this case the maximum stroke of the press is 25mm. that is why for the deep drawing the length of the sides of the square box is limited to 50mm.

Now if we take into the consideration of the drawing force equation there are two things which can be very C and R. By taking the both the extreme values of the h/R ratio better result is obtained by the taking $h/R=2$ in this case.

Also other thing which has to consider is the radius at the bottom of the punch r, because for both Rc and length $(h + \Pi r/2)$ the common parameter is r value. So r should be such that there is minimum difference between the Rc and $(h + \Pi r/2)$ and also there is the limiting value of the r which is between $3\text{-}8r$. So considering all these effect the results are shown in the table 3.2.

L	50*mm*
Rc	27*mm*
X	32*mm*
R	12.5*mm*
C	0.5
h/R	2
R	4.5*mm*
Ft	110 *N/mm2*
Vdr	1.2 tonnes.

Table 3.2: List of the input parameters for blank geometry

These are the parametric values founded from geometric relation without considering the plasticity effect of the material and trimming allowance. This initial blank size will be optimized after the initial numerical solution.

For carrying out the initial numerical solution of the process the values of the other parameters of the die and punch is shown below.

- For the general calculation value of die radius should be taken as $4<=\rho/t<=10mm$.As here thickness is 1 *mm* so die radii should between $5<=\rho<=10$ *mm*. It is taken as 10*mm*. That will be optimized by taking different die radii.
- Punch radius is considered as 4.5 *mm*.
- Normally the value of punch and die clearance is taken as *1.15t to 1.20 t*. But as aluminum is used so clearance is provided equal to the stock thickness or 1mm.

In the above section all the geometrical data required for the modeling is calculated. After initial FEA simulation that geometrical parameter or blank dimensions is optimized. Drawing force calculated is without considering material stretching, friction between contacting surface and thickness variation of the sheet so, actual drawing force will be more than the calculated.

3.6 Determination of the Roff value.

3.6.1 Methodology

1. Calculation of geometric size and other normalized parameters k, S, p, C_p.
2. Normalized cup forming depth P_d by the size s and drawing ratio factor k.
3. Value of the central strain and coefficient of friction according to the requirement of the part.
4. Calculate the normalized roff value used in the 2d model.$r_{off}^{2D}=r_{off}$ S.
5. Build the 2d geometry model according to the geometry of the part and calculate r_{off}^{2D} value.
6. Run the 2D model with various binder forces until the forming depth $y_p^{2D}$is obtained.$y_p^{2D}=y_p$ k.
7. Finding the binding force to be used in the 3D forming process by this equation [14].

$$F_b^{\,e} = \frac{Fb(A_2 + A_4)(R_{off} + r_s)\theta}{2\pi(A_1 + A_2 + A_3 + A_4)r_s}$$

3.6.2 Determination of the binder force with the above method.

Fig: 3.2 the plane view of the geometry. Forth part of the model is taken for the calculation of the R_{off}

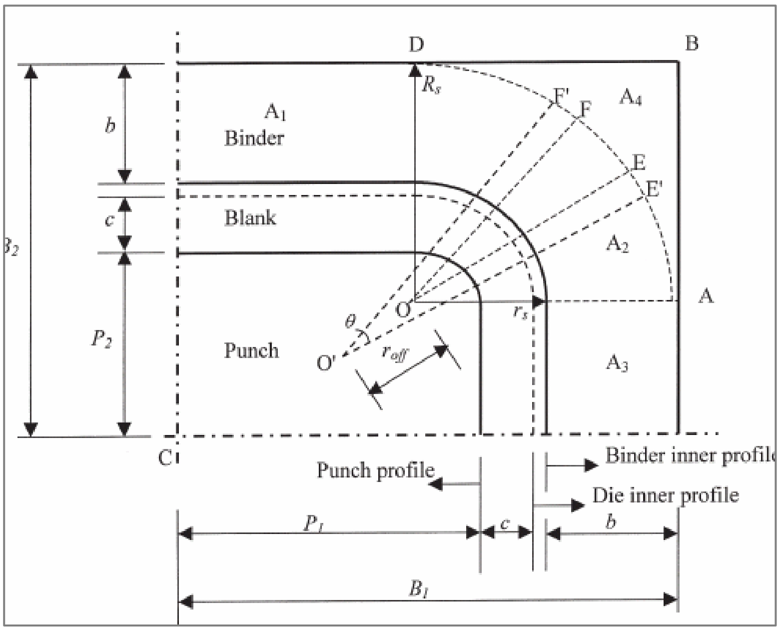

Fig: 3.2 General schematic diagram of components

In the above fig: 3.2 plan view of the geometry is given. Initial is divided in to the four zones. As above schematic diagram is for the base model so actual model have to normalized, which is shown below:

1. General problem that must has to be standardized with the base model.

   d_1 and $d_2 = B_1/P_1 = 2.08$.

   $k = d_1 d_2 / d_0 d = 0.98$.

   $S = kB/B_0 = 0.98\ (B/B0)$

   $Cp = c/P = 0.041$

   $p = (P/P_0)\ S = 1.0549$.

   $y_p = (p_d/s)k = 37.69$mm.

2. Now as generalized parameters are calculated that will be input to the r_{off} function [14].

$$\boxed{R_{off} = \frac{0.358 FLD^{2.1286} k^{1.3853}}{\varepsilon_c^{1.4106} p^{4.2318} y_p^{0.4334} c_p^{0.6411} \mu^{1.0643}}}$$

3. By putting different values from the generalized taking value of $\varepsilon c = 0.005$ and value of coefficient of friction equals to 0.04 r_{off} value is determined as 16.77mm or we can say 17mm.

4. By putting these in to the equation of binding force the value of the binder force is coming around 1800 to 2000 N.

   Where, $A_1 = A_2 = A_4 = 625\text{mm}^2$ $A_3 = 572.55\text{mm}^2$

Approximate value of blank holding force determined by above method is 1920N. That can be very depending on the other parameters.

Here blank holding force, drawing force and the initial blank size are calculated, which are the initial requirements of the deep drawing process. Approximate calculation of the blank holding force can reduce the trial and error time in the FEA simulation.

In the next chapter FEA simulation of the deep drawing process is carried out. Methodology and results showing the strain pattern is given in the next chapter. Results and flow limit curve of the three different blank shapes are shown.

CHAPTER 4

FEA simulation of square cup using ANSYS-LSDYNA

4.1 Introduction

In this chapter theoretical back ground for FEA simulation, procedure for the simulation, and results of the simulation using three different initial sizes of the blanks are included. Explicit dynamic analysis is carried out for the simulation. Results of Major strain, Minor strain, Von mise's equivalent stress and flow limit curve for the process are included.

4.2 Theoretical background for the numerical simulation

4.2.1 Introduction

Deep drawing is a very complicated process in which the plastic flow of the material takes place. Material non linearity, dynamic behavior of the tool and contact between the blank and other parts like blank holder, punch, and die is the area of the concern. Theoretical part of things like type of the elements used for the blank, contact conditions, blank holding force, adaptive meshing, material model used in the simulation is should be considered for the better simulation results. Velocity of the punch or we can say the input velocity curve and load curve which is applied at the time of loading which shows the forces at the time of impact. So we can say that it is dynamic process and we have to consider each and every parameter that may affect the process. Here is the theoretical background for the numerical simulation.

4.2.2 Element (SHELL 163)

There are many formulations are available for the shell 163. In this simulation belytachko-T say membrane is considered. It is fast and recommended for most membrane element applications, reduced one point integration and good for fabrics where wrinkling is concern (i.e where large in-plane compressive stresses try to collapse the thin fabric elements).

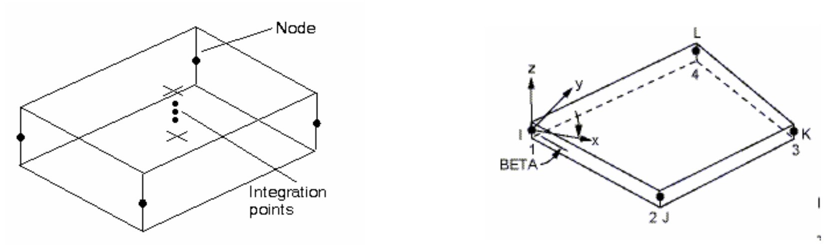

Fig: 4.1 Integration points of SHELL 163 element.

The Belytachko-T say membrane shell element (fig: 4.1) is based on a combined co-rotational and velocity strain formulation. The efficiency of the element is obtained from the mathematical formulation simplified by result from the kinematics assumption. The co-rotational portion of the formulation avoids the complexity of the non-linear material mechanics by embedding a coordinate system in the mechanics.

4.2.3 Contact control (surface to surface)

Friction model in LS-DYNA is based on a column formulation. The friction algorithm, outlined below, uses the equivalent of an elastic spring.

- Compute the yield force.
- Compute the incremental movement of the slave node.
- Update the interface force to the trial value.
- Check the yield condition.
- Scale the trial force if it is too large.

The interface shear stress that develops as a result of the column friction can be very large and some cases it exceeds the ability of the material to carry such stresses. Forming contact (FSTS) is used in metal forming applications. For these contact types, tools and dies are typically defined as target surface and blank as slave surface.

4.2.4 Adaptive meshing.

In metal forming analysis, a body may experience very large plastic deformation. Single point explicit element which is usually robust for large deformations, it may give accurate results in these situations due to inadequate element aspect ratio. So counteract that problem LS-DYNA has adaptive meshing.

4.2.5 Material model.

Barlat's anisotropic plastic model is used for material model in forming processes. The yield function ***Φ*** is defined as:

$\Phi = (S1\text{-}S2)^m + (S2\text{-}S3)^m + (S3\text{-}S1)^m$

$Sxx = (1/3)[c(бxx\text{-}бyy)\text{-}b(бzz\text{-}бxx)]$

$Syy=(1/3)[a(бyy\text{-}бzz)\text{-}c(бxx\text{-}бzz)]$

$Szz= (1/3)[b(бzz\text{-}бxx)\text{-}a(бyy\text{-}бzz)]$

$Syz=f\ бyz$

$Szx=g\ бzx$

$Sxy=h\ бxy$

$бy= k(\varepsilon^p + \varepsilon_0)^n$ ……………………………………………………(8)

Where *a, b, c, h, g,* f are anisotropy material constant and k, n, ε^p, ε_0 are strength coefficient, strain hardening coefficient, Plastic strain and initial strain coefficient respectively.

4.2.6 Rigid bodies.

In the deep drawing die and punch is the fix part and punch will move in the vertical direction with constant velocity. The punch, die and blank holder are harder than the blank material it is considered as the rigid body because it saves simulation time required for the process. Initial velocity, loading curve and other constraints is transferred to the c.g of the rigid body from any other node.

Using rigid bodies to define stiff parts in finite element model can greatly reduce computational time required to perform an explicitly analysis. When rigid bodies are defined, all degree of freedom of the nodes in the rigid body are coupled to the body's center of mass. Hence, rigid body has only six degree of freedom regardless of the number of nodes defining it. By default mass center of the body and inertia of the body is calculated from the density of the element.

For the explicit dynamic analysis above terms are critical and input value to that affects the end results. Like contact condition and adaptive meshing is very critical. So, theoretical background is necessary for this process. The next section, procedure for the simulation and modeling and meshing are given.

4.3 Procedure for the FEA simulation.

Below some of the steps are shown to carry out numerical simulation.

- Modeling of components in the Pro/E wildfire 2.0.
- Importing the model in the ANSYS LS-DYNA.
- Modifying the imported geometry in the ANSYS by using the preprocessor7.
- Applying material model by considering punch, die, and blank holder as the rigid bodies.
- Meshing of all the components with the SHELL 163 (Belytachko-T say membrane) element.
- Applying constraint to the components. Die is constrained with all displacement and rotational direction. Punch and blank holder are constraint by all rotation and displacement in the z and x directions.
- Apply displacement constraint to the punch in y- vertical direction.
- Apply initial velocity and load curve to the one node of the punch and berth and death time for the load curve.
- Apply forming surface to surface contact (FSTS) by considering die, punch and blank holder surface as target surface and blank as contact surface.
- Mass scaling of the blank to reduce the time required for the simulation.
- Apply adaptive meshing to the blank.
- Apply time required for carrying out the simulation (termination time).
- Solution and the plotting of the results.

Above are the basic steps for carrying out analysis. There are input parameters for the material models are given in the appendix A. In the next section modeling and meshing are shown.

4.3.1 Modeling and meshing of the components.

Fig 4.2 Shows model created in pro/e wild fire 2.0. And dimensions are taken as calculated in the chapter 3. In the fig 4.2 general modeling is shown, which includes basic component of the deep drawing process.

Die radius and punch radius are taken as 5mm. Clearance between die and punch is taken as 1mm or stock thickness. The thickness of the blank is taken as 1mm. Die radius at the corner in the plane view is taken as 8mm. Punch radius in the corner in the plane view is taken as 10mm. This model is saved as surface model in the IGES format.

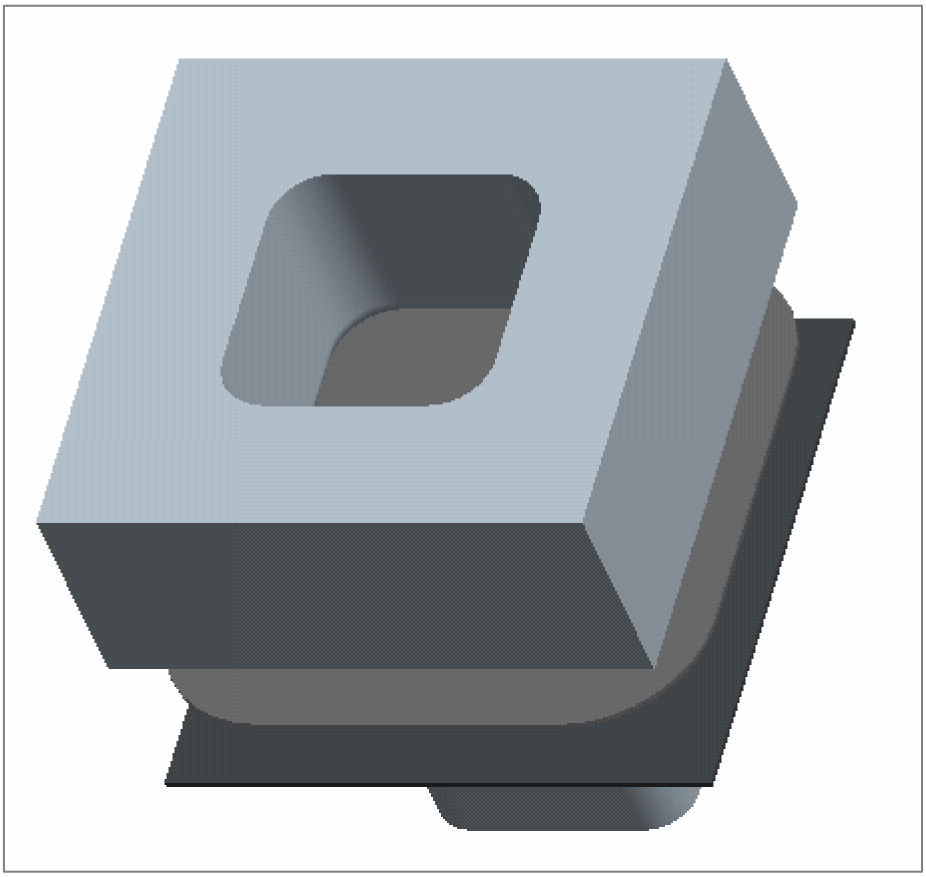

Fig: 4.2 Modeling of the components.

4.3.2 Meshing and modification of the components in ANSYS.

The imported geometry from the proe/ wildfire-2 is modified in the ANSYS. Surface model is generated in the ANSYS by removing the unnecessary areas. Modified geometry is shown in the fig: 4.3, which shows only the surface area of the components.

Meshing of the components is shown in the fig: 4.3. Die, punch and the blank holder are defined as rigid bodies for reducing time required for the simulation size of the element is not concern for those parts. So meshing of those components remains same for all the simulations. Meshing of the blank are changed according to the initial shape of the blanks. Those are shown in the respective simulations.

(a) **(b)**

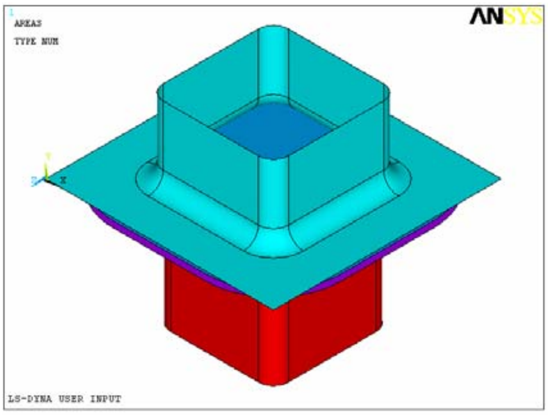

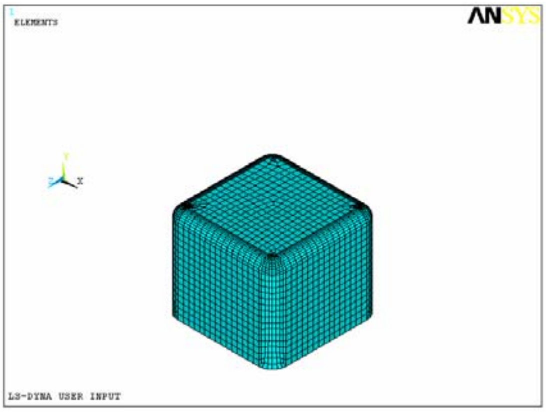

(c) **(d)**

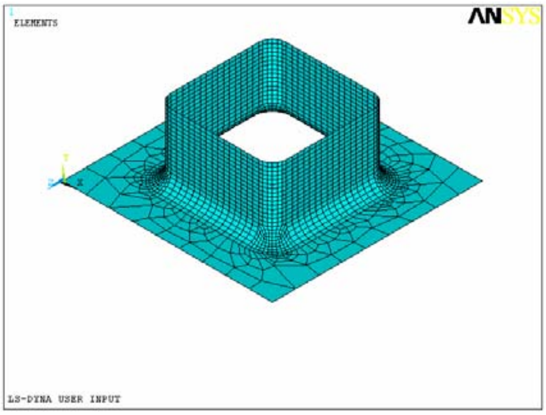

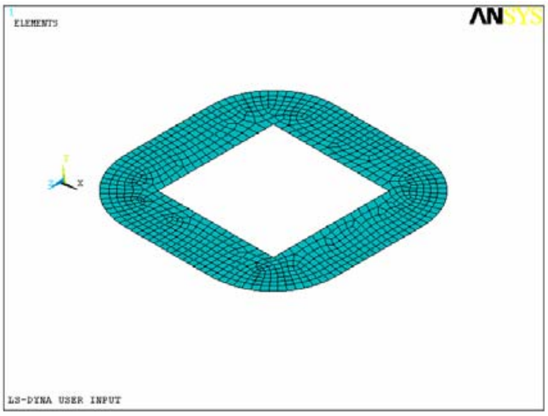

Figure 4.3 (a) Modeling of the components, (b) Meshing of the Punch, (c) Meshing of the die (d) Meshing of the blank holder

4.3.3 Loading and boundary conditions.

There are generally two methods are used for getting the displacement of the punch in the vertical direction. We can directly apply the displacement to the punch as rigid body and we can also apply the velocity curve or called as load curve to the punch. Actual maximum velocity required for the deep drawing of the process is approximately 750mm/sec. But for reducing the simulation time virtual velocity of 1500-2000mm/sec is applied to get the required displacement to the punch. In the fig: 4.4 velocity curve is shown for the termination time of 0.01 sec.

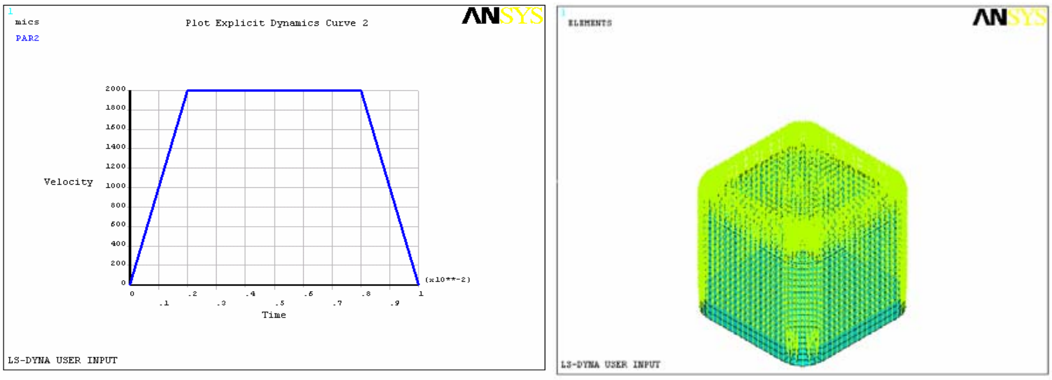

Figure 4.4: Velocity curve for the punch

Important thing in the FEA simulation of deep drawing is the application of the blank holding force because at the time of the punch deforming the blank sheet material blank holder must be start applying force on to the blank. For that load curve showing the gradual increase in the load at the start of the process and meet the blank just prior to the punch touching the blank is applied. Fig: 4.5 Shows the load curve for the blank holder.

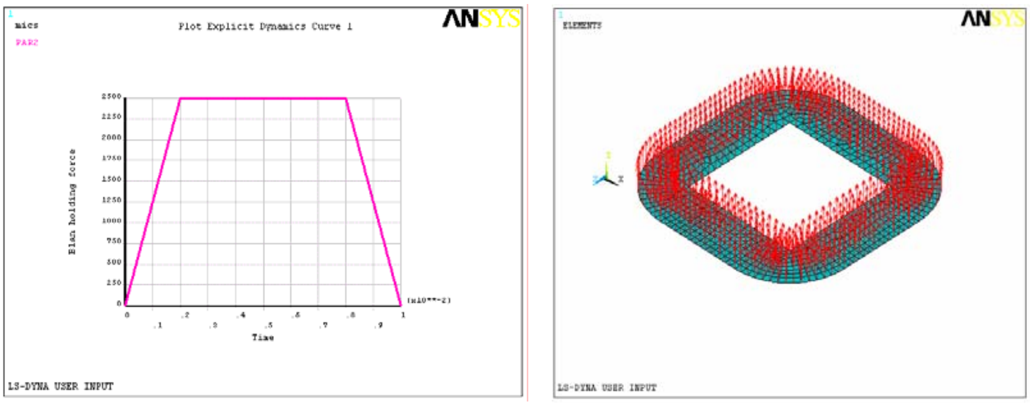

Figure 4.5: Load curve for the blank holder

4.3.4 Constraints applied to the die punch and blank holder

Die is constrained in all the rotation and translation directions. Punch and blank holder are constrained in the Z and X translation direction and fully constrained in the rotational direction. So punch and blank holder are allowed to move in the Y or vertical direction.

4.3.5 Mass scaling

Proper use of the mass scaling will add a small amount of mass to the model and slightly changes a structure, center of mass. Use of the proper mass scaling reduces the total CPU time. For the application of the mass scaling minimum time step size is required, which can be calculated form the equation given below.

$$\boxed{\Delta t_{\min} = \frac{l_{\min}}{c}}$$

Where, $l_{\min}$ is the min. length of the element and c is the sonic speed.

$$\boxed{c = \sqrt{\frac{E}{(1-\gamma^2)\rho}}}$$

After doing the above steps surface to surface contact was applied to the blank to other components, which is based on the penalty based algorithm. The blank was taken as slave surface and other surfaces were taken as target surface.

All these procedure shown above are the general procedure, which shows the outline of the input parameters required for the simulation. Specific inputs for the each of the simulation case are mentioned in the respected simulation.

4.4 FEM simulation of square cup of aluminum 1100.

4.4.1 Introduction

For the simulation of the Square cup punch nose radius and die edge radius are taken as 5mm. The simulations were carried out by taking three different shapes of the blanks. General procedure for the simulations is described in the above section. In this section results of the Von mises's stress, Major and Minor strain produced in the drawn cup and flow limit diagram for the each case are included. Macro created in APDL is used to carry out the simulations.

4.4.2 FEA simulation of Square cup with Square blank of size 100x100.

The general geometrical data is described in the modeling section. fig: 4.6 Shows the meshing of the component with the element size is equal to 2 . The load curve will be of the same shape that has been described in the earlier section. Material data for the Barlat's model is given in the appendix A. Load curve for the 2300N is applied to the blank holder. Velocity curve for the punch applied as described in the previous section of the 2000mm/sec.

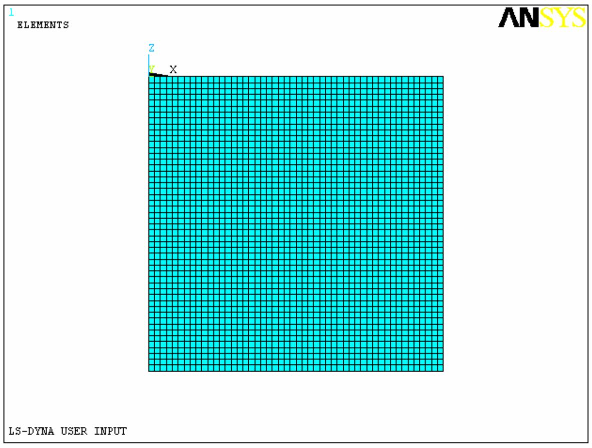

Fig: 4.6 Meshing of the square blank, Aluminum (1100)

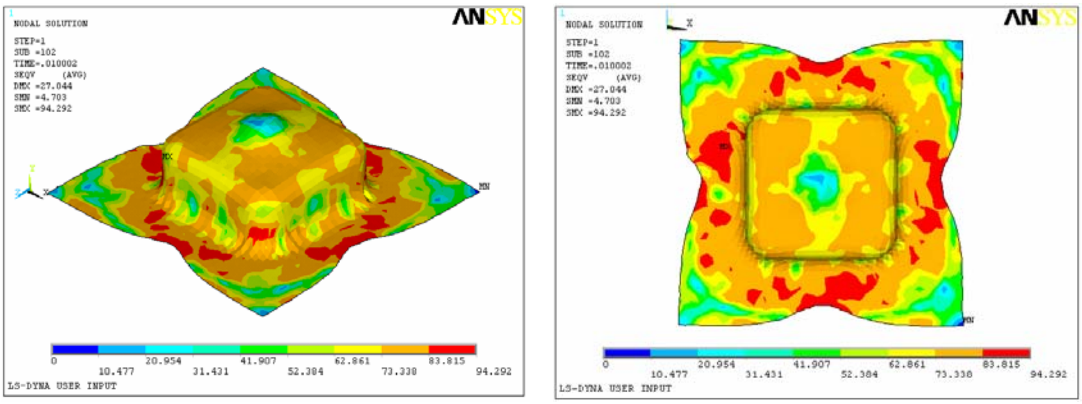

Fig: 4.7 Von mises's equivalent stress in square blank (Aluminum 1100)

Stress value in the critical region is around 94.292 N/mm^2 which is below the ultimate strength ($108N/mm^2$). The yield strength of the material is $80N/mm^2$. So stress value is within permissible limit. Also stresses at the region near the flange of the side wall are higher due to the blank holding force, because blank holding force area is higher at the corner and less at the side wall region.

Fig: 4.8 Shows the results of he Major strain produced in the part, because the fate of the deep drawing is generally decided by the Major strain.

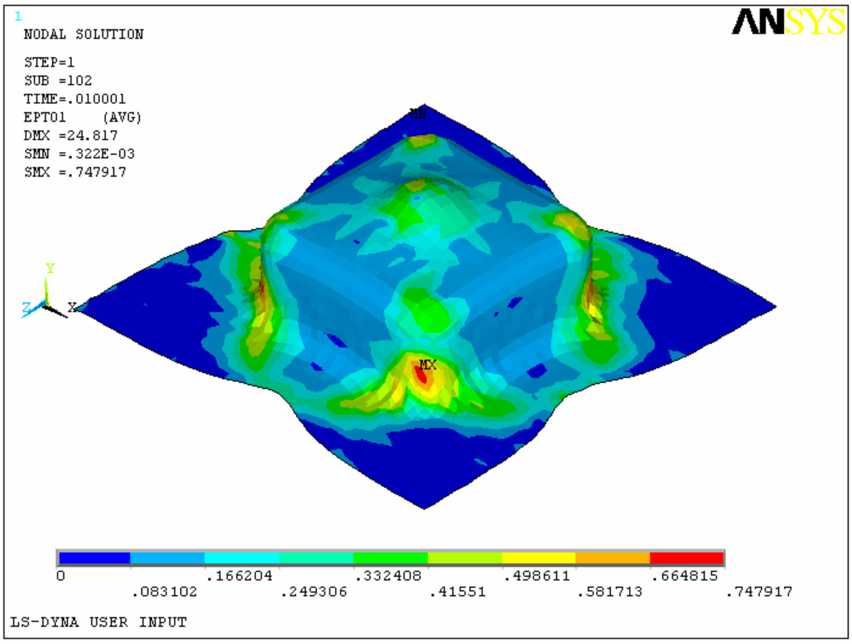

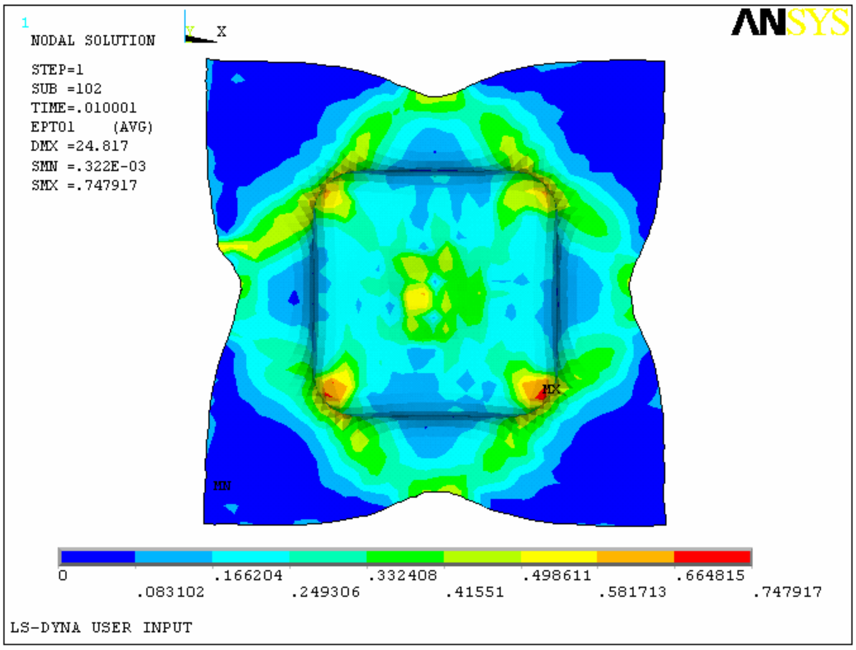

Fig: 4.8 Major strain produced in the drawn cup from the square blank. (Aluminum 1100)

Fig 4.8 shows that strain value in the region just below the die radius is higher, which is 0.747917 and around that region it is be 0.581713 to 0.6648. which are in the safe region of the die corner. So from the above strain values it can be said that the chances are there for the cup to fail around that region if strain is higher than 0.75. It is also observed that the maximum stress strain pattern is spread just below the die radius and around the region where flanges of the side wall and corner is connected.

Fig: 4.10 Shows the minor strain produced in the cup. As like the major strain it one of the critical result, which decides the fate of the deep drawing process. Minor strain in combination with major strain decides the strain pattern produced in the component.

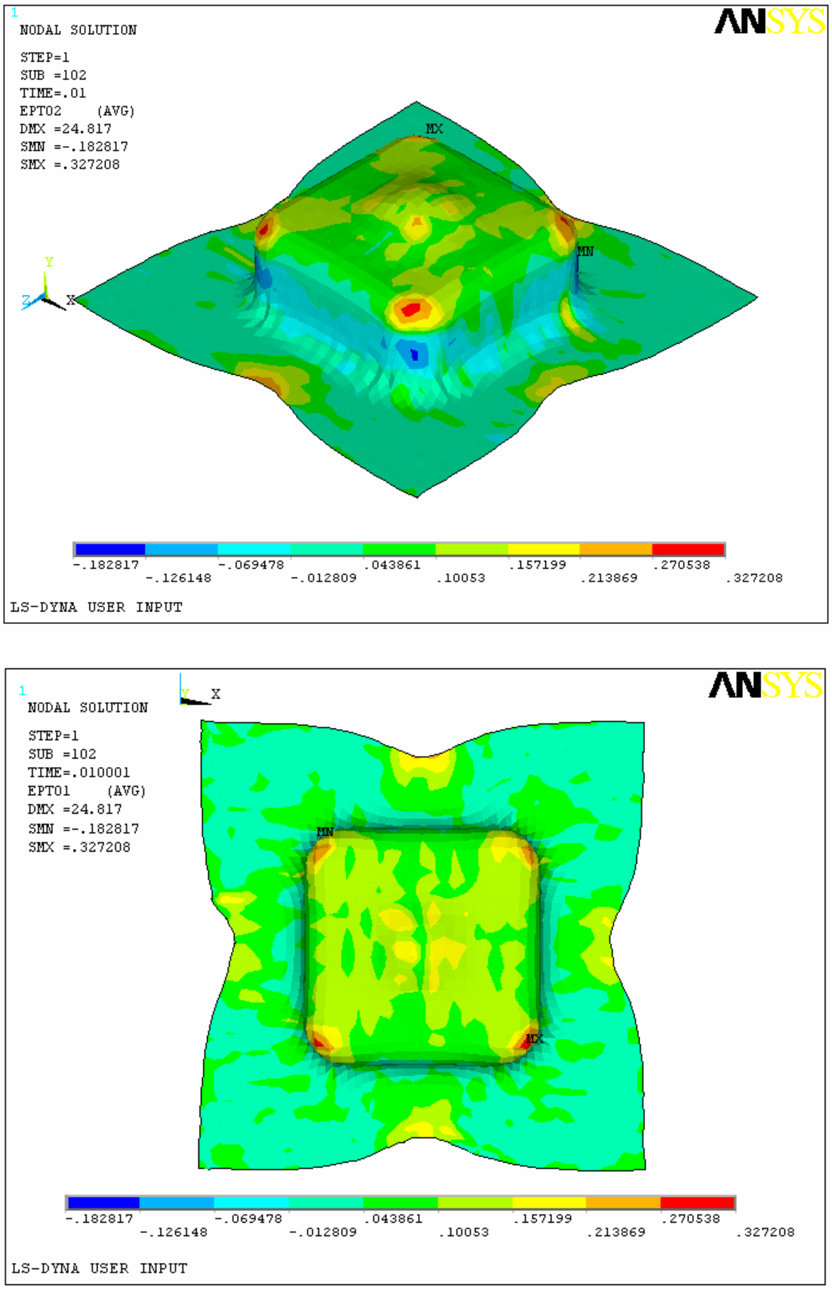

Fig: 4.9 Minor strain produced in the drawn cup from square blank (Aluminum 1100)

Fig 4.9 Shows the minor strain in higher in the region of the punch radius, that is because of the bending and stretching both occurs in that region. In that region both minor and major strains are of tensile in nature.

In the zone just below the die radius, which are having minor strain of the compressive nature, which shows the nature of the deep drawing. That is the region where Major strain is of tensile in nature and minor strain compressive in nature.

Fig: 4.10 Shows the flow limit diagram. The nature of the deep drawing can be investigated by this diagram. It is a plot of Major Vs Minor strain.

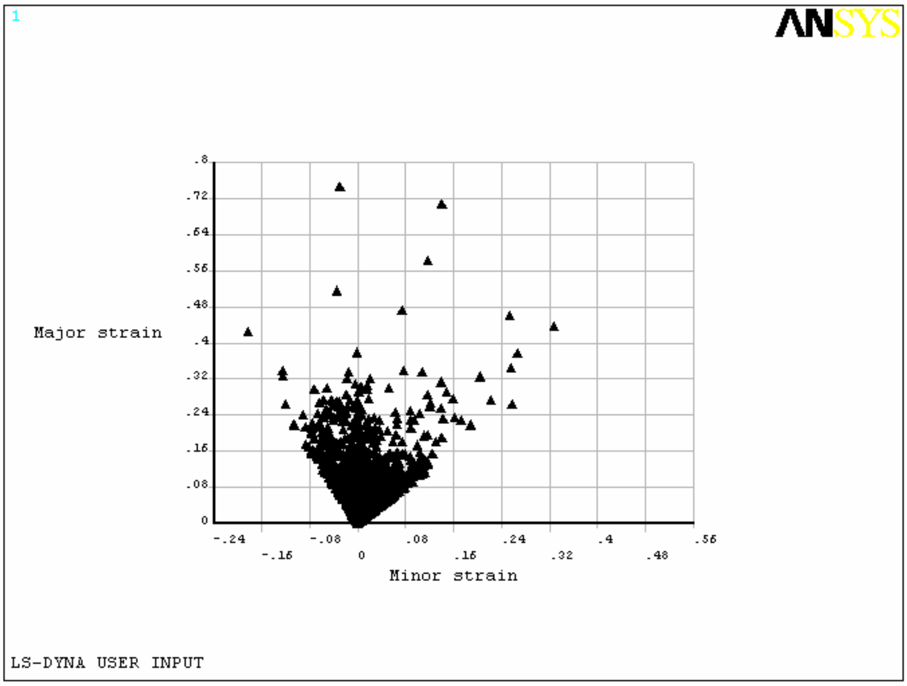

Fig: 4.10 Flow limit diagram for the drawn cup from the square blank. (Aluminum 1100)

Fig 4.10 shows that the some of the points are nearer to the plane strain condition and major strain is higher at that point, that can be the point at which failure occur. Other points are falling below the safe line which, at the plane strain condition is 0.38. Some of the point are falling in the just the below the region of safe region and plane strain condition where chances of wrinkling are very less. That was on the left side. On the right side of the graph, stretching of the metal in the both direction indicates the points which are nearer to the punch nose radius. And values are coming in the safe region. So it can be said that the critical region is just below the die radius where maximum value of the major strain is 0.74.

4.4.3 Square blank of size 100x100 with corner radius of 22mm.

Square blank with corner radius of 22mm is deep drawn into the square cup. The material and other input parameters remain same for the process. The load curve and the velocity curve are taken as given in the earlier section. Only the shape of the blank is changed. Element size is taken same as 2. Fig: 4.11 Shows the meshing of the blank.

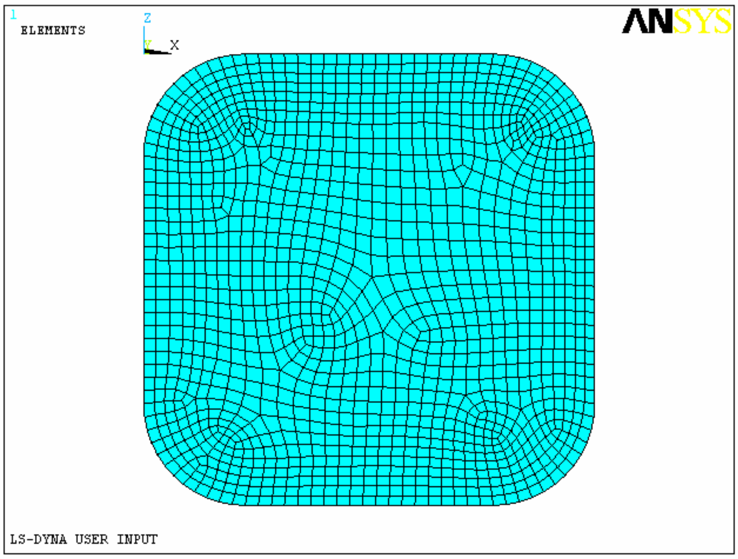

Fig: 4.11 Meshing of the square blank with corner radius 22mm. (Aluminum 1100)

Fig 4.12 shows the Major strain produced in the drawn cup. Same as in the above case one of the deciding results is the Major strain but as other parameter other than shape remains constant. But binder force area is decreased.

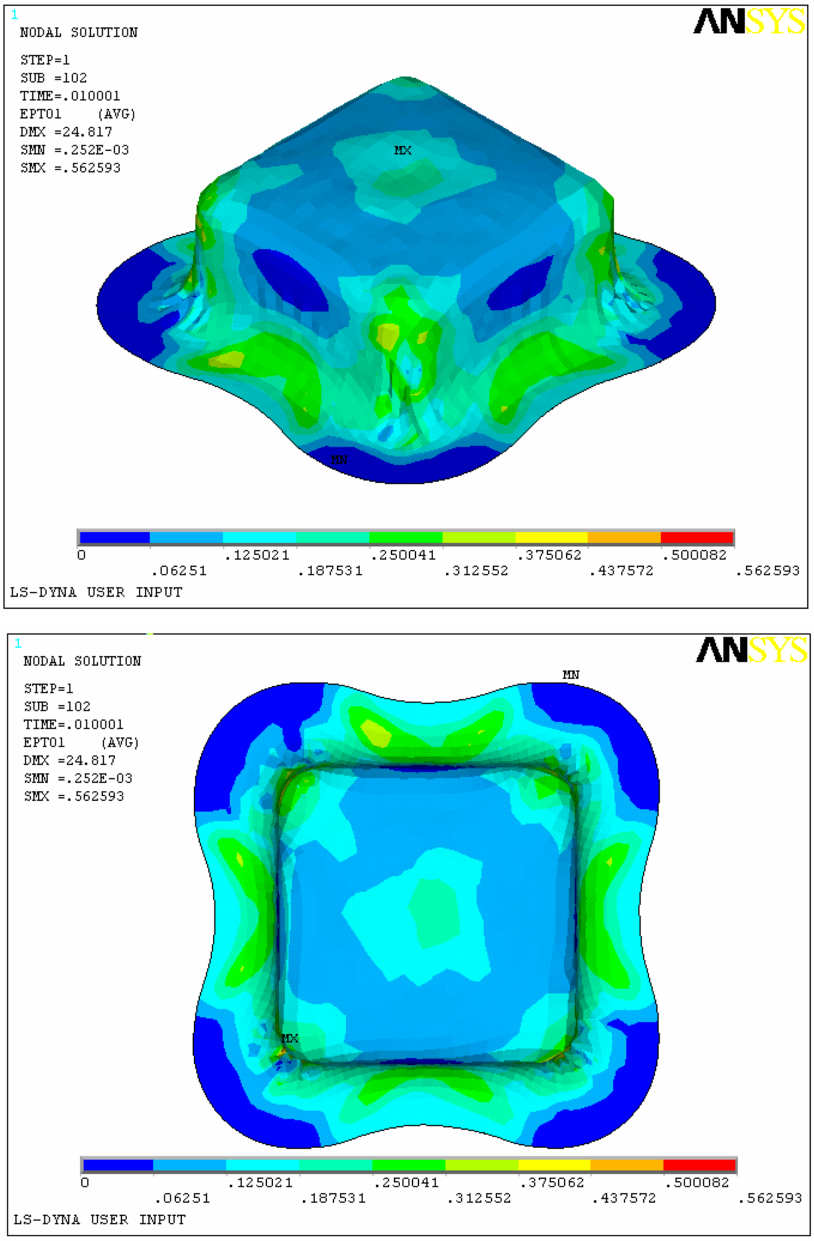

Fig: 4.12 Major stress produced in the square blank with the corner radius of 22mm. (Aluminum 1100)

Fig: 4.12 Shows that the maximum strain value is around 0.5629 which is good for the deep drawing. Generally, the maximum value of the major strain comes around that value. The results shows the lower value of the stresses around the die radius than at the punch, so at can be said that the chances of failure are very less in any of the region. And other pattern around the flange of the side wall is similar fashion that generally with the other case.

Fig: 4.13 Shows Minor strain produced in the blank.

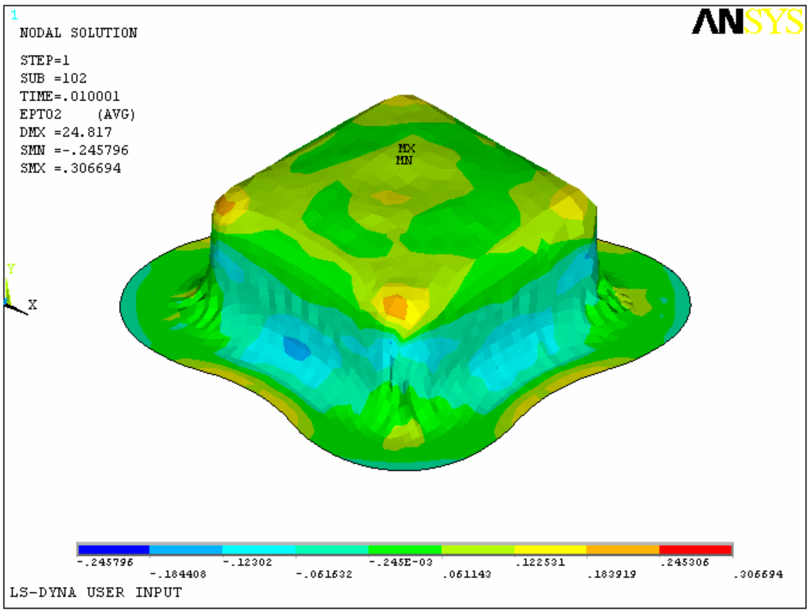

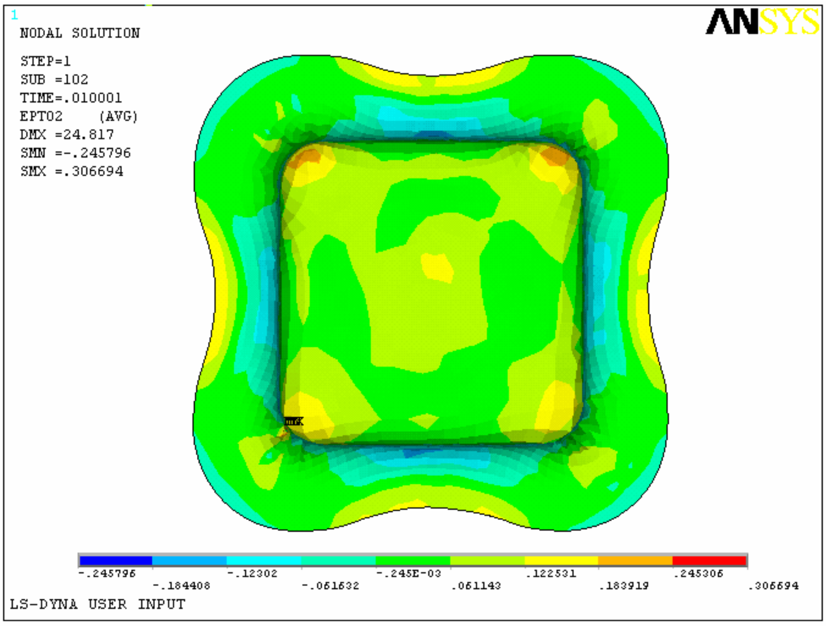

Fig: 4.13 Minor strain in the square blank with corner radius of 22mm. (Aluminum1100)

Fig: 4.13 shows that the maximum value of the Minor strain is around 0.3066 which is quite law and that around the punch nose region. As the major strain is quite low in the component the value of the minor strain is mostly positive in nature which indicates uniform distribution of the strain. So from above results of the strain in the critical region flow limit diagram is plotted, which is shown in the Fig 4.14

Fig: 4.14 Shows the flow limit diagram of the process, which is Plot of Major strain Vs Minor strains produced in the blank. The deep drawing of the process is investigated by the points falling in the left side of the graph, where Major strain positive in nature and Minor strain is compressive in nature.

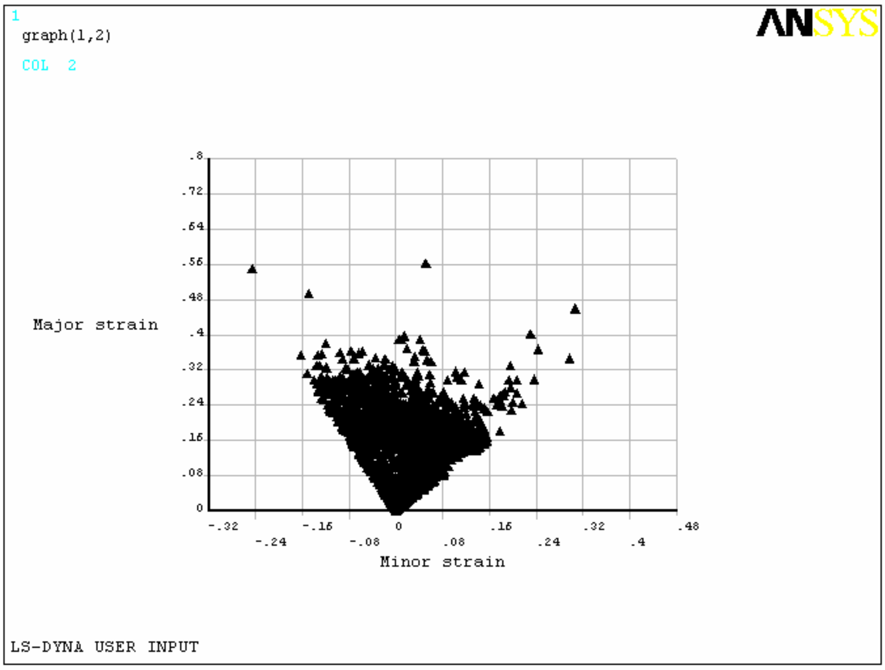

Fig: 4.14 Flow limit diagram for the square blank for the corner radius of 22mm

Fig 4.14 Shows that at plane strain condition value of the Major strain is 0.39, which is the safe value. Also points are not falling in to the wrinkling zone on the left side which indicates no wrinkling of the sheet. One or two point on the right side of the graph is just on the boundary of the slope but that is within the safe zone.

4.4.4 FEA simulation of square cup with circular blank of 100mm size. (Aluminum 1100)

Circular blank of 100mm diameter is deep drawn into the square cup. The material and other input parameters remain same for the process. The load curve and the velocity curve are taken as given in the earlier section. Only the shape of the blank is changed. Element size is taken as 3. Fig 4.15 shows the meshing of the blank.

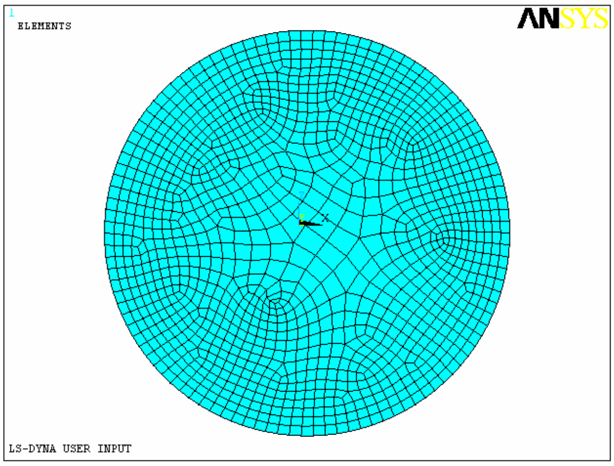

Fig: 4.15 Meshing of the circular blank of 100 mm diameter. (Aluminum 1100)

Fig: 4.16 Shows the Equivalent Von mises's produced in the circular blank.

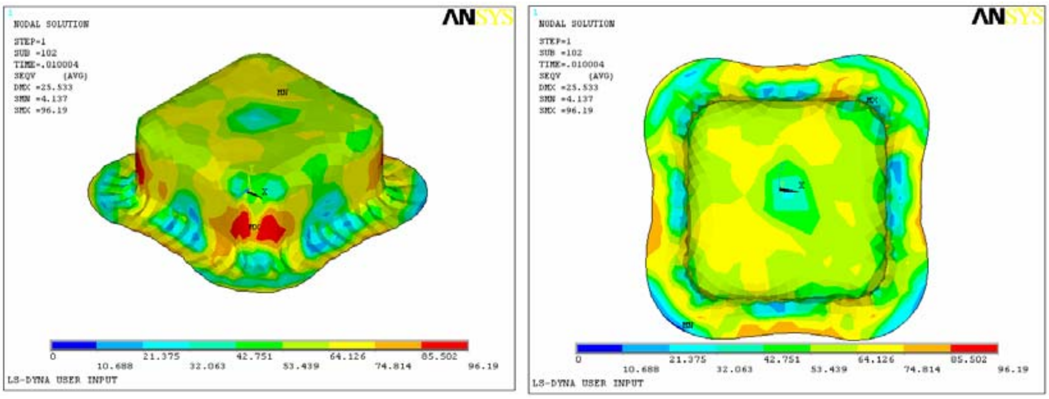

Fig: 4.16 Von mises stress drawn cup from the circular blank. (Aluminum 1100)

Fig: 4.16 Shows the maximum value of the stress is 94.39/N/mm^2 is less than the ultimate stress (108 N/mm^2). It is higher in the region just below the die radius. Material is stretched around just below the wall of the die radius and due to that value is higher in that region.

Fig: 4.17 Shows the Major strain in the drawn cup from the circular blank.

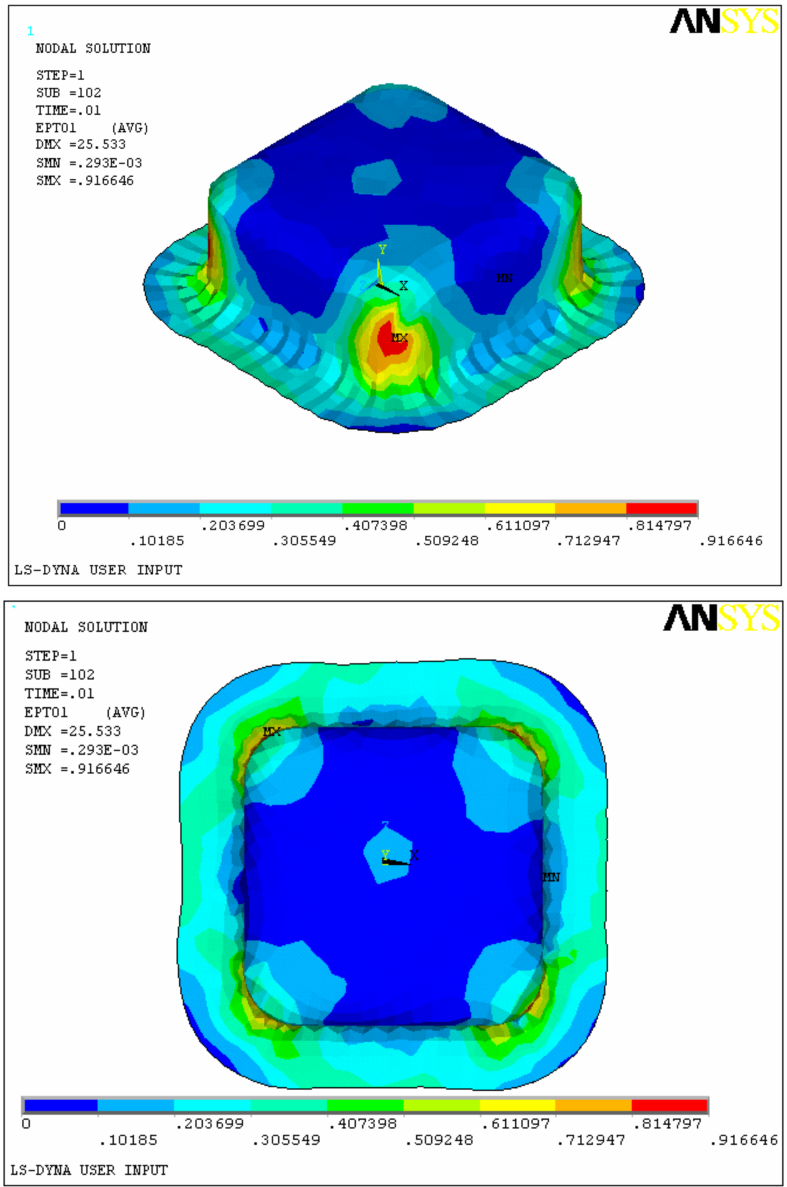

Fig: 4.17 Major strain produced in the circular blank. (Aluminum 1100)

Fig: 4.17 shows that maximum Major stain 0.99 in the part is at just below the die corner radius. The other region it is within the safe limit. Wrinkles are also observed in the flange region, which always the case with the circular blank. Blank holding area in the circular blank is lower compare to the other two cases so the amount of wrinkles are higher in that region. Region at the side wall flange region is also stretched so strain is uniformly distributed in that region.

Fig: 4.18 shows the Minor strain produced in the deep drawn square cup.

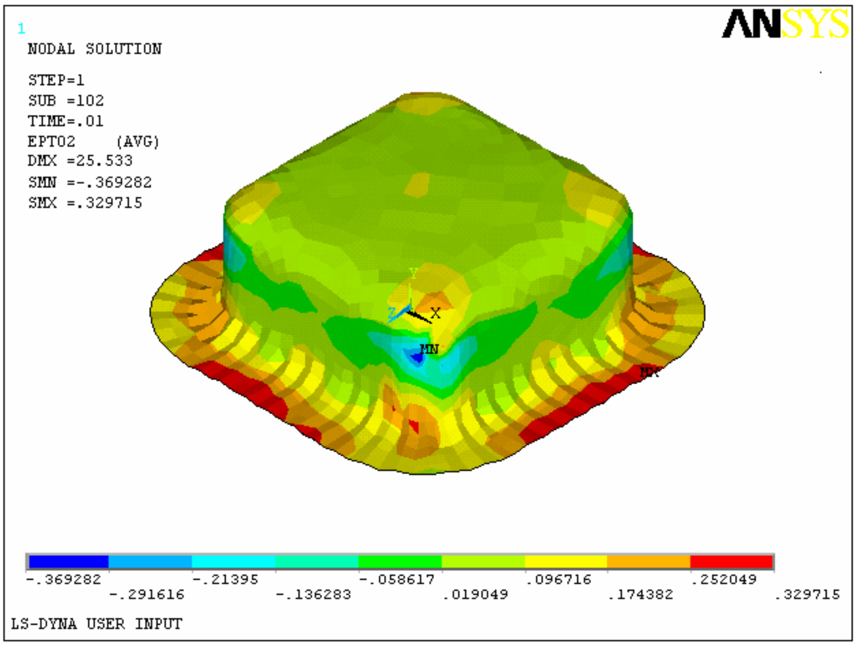

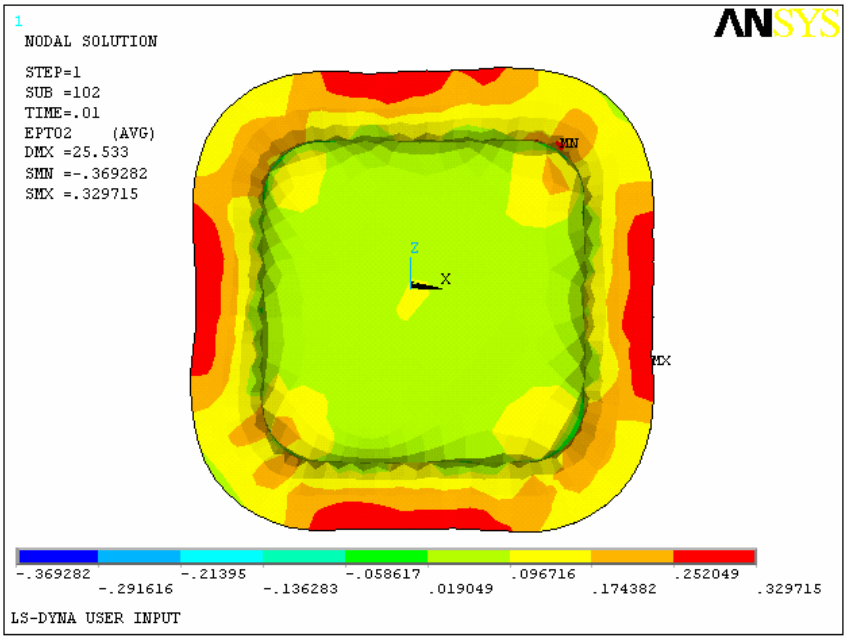

Fig: 4.18 Minor strain produced in the circular blank. (Aluminum 1100)

Fig: 4.18 Shows that the Maximum value of the Minor strain is 0.329 and that is around the flange of the side wall. That is because of the restraining force applied through the corner. Compressive strain is in the area where major strain higher. It is the region where true deep drawing process takes place. Minimum value of the Minor strain is -0.3692.

Fig: 4.19 Shows the flow limit diagram of the deep drawn part.

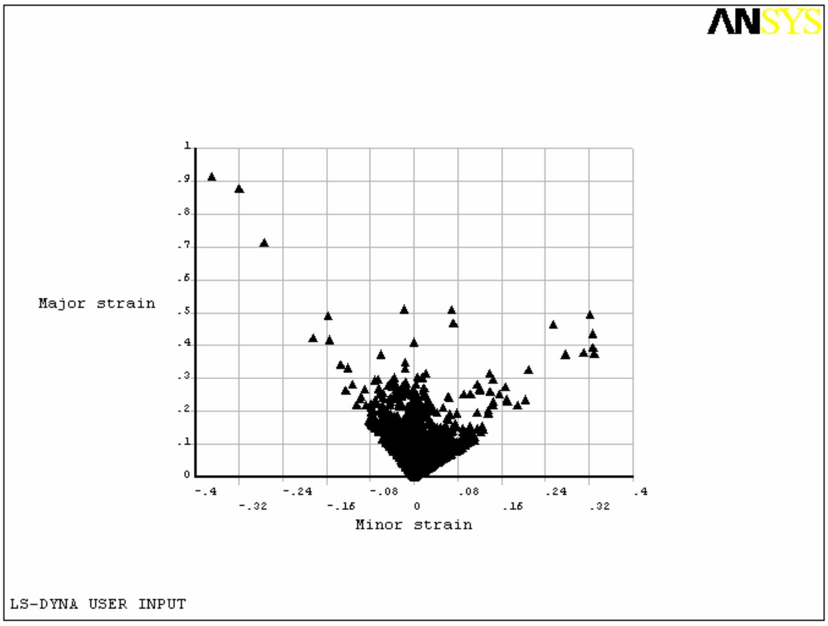

Figure 4.19: Flow limit diagram for the circular blank. (Aluminum 1100)

Fig: 4.19 Shows that the at the plane strain condition the value of the major strain is 0.43. Some of the points are falling in the wrinkling limit region. So it can be said that higher blank holding force is required to remove the wrinkles but as the value of the strain is higher just below the die radius increase in the blank holding force can fail the part in that critical region. So proper application of the blank holding force can reduce the wrinkles and strain in the component.

All the above simulations are carried out with the use of Macro in APDL to reduce the time required for the iteration. This methodology of the simulation can be applied to the other materials also. In the next section same methodology of the simulation ids applied to the Aluminum 5052 square cup with the initial size of the blank calculated in chapter 3.

4.5 FEM simulation of square cup of aluminum 5052.

4.5.1 Introduction.

The simulations are carried out for the 5mm and 8mm die radius. Clearance between die and punch is provided as 1.15mm. Punch radius is taken constant as 5mm. Input parameters for the Barlat's material model is given in the appendix A. The initial blank size for the simulation is taken as modeled in the chapter 3. Input velocity curve is taken same as defined in the earlier section. The simulations are carried out with use of Macro developed in APDL.

4.5.2 FEM simulation of square cup of aluminum 5052 for the die radius of 8mm.

The simulated results for the die radius of 8mm are carried out. As this is harder material the strength of material is higher. So that requires higher bending radius for the process. The blank holding force is very I the region between 3700N to 4000N to get the required shape.

Fig: 4.20 Shows the Von mises's equivalent stress produced in the cup.

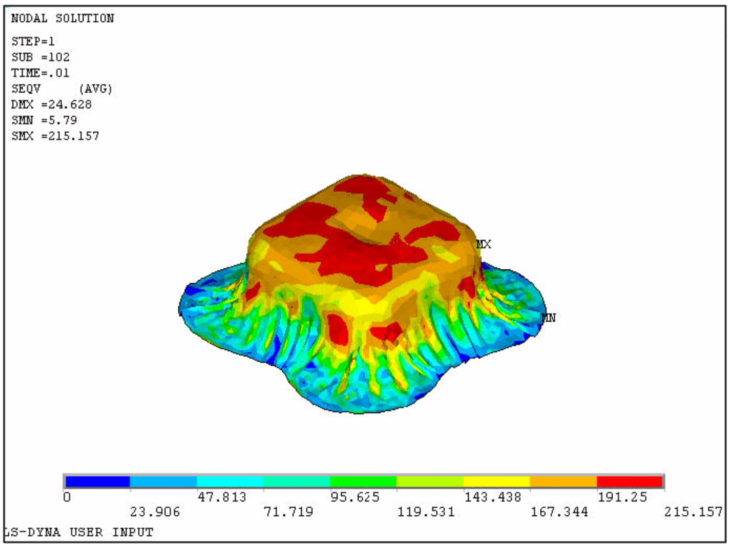

Fig: 4.20: Von mise's equivalent stress produced in square cup (Aluminum 5052), Die radius 8mm.

Fig: 4.20 Shows that the stress produced in the blank is higher in the wall between die and punch radius. The maximum stress produced is 215.157 N/mm^2 which is higher than the ultimate stress (265 N/ mm^2) of the material. So it can be said that it is yielding at the critical region but within the limit of the ultimate stress.

Fig: 4.21 Shows the Major strain produced in the blank.

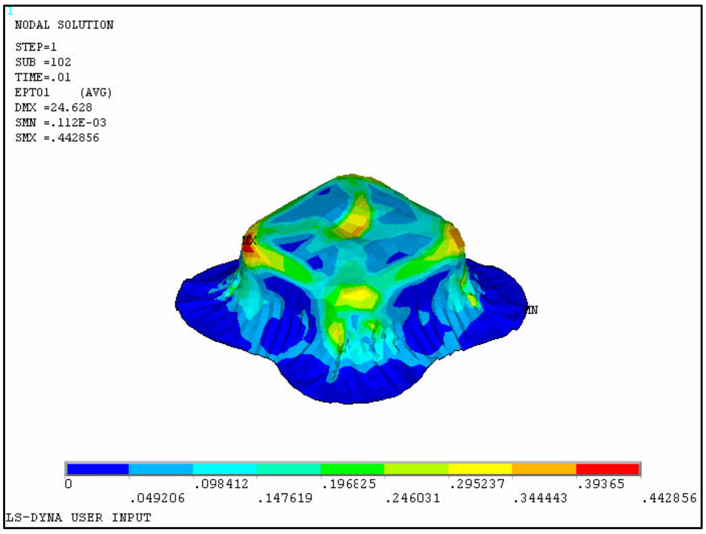

Fig: 4.21 Major strain produced in square cup (Aluminum 5052), Die radius 8mm.

Fig: 4.21 Shows that maximum value of the strain is in the region of the punch nose and it is 0.4428. As die radius is 8mm the force required to draw the material is less and that is producing lower strain in the die region.

Fig: 4.22 shows the Minor strain produced in the square cup.

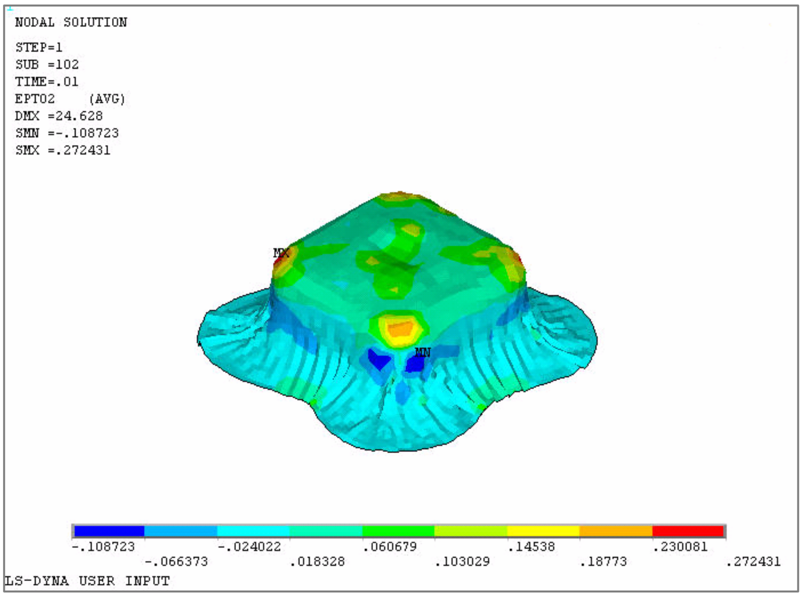

Fig: 4.22 Major strain produced in square cup (Aluminum 5052), Die radius 8mm.

Fig: 4.22 Shows that the value of minor strain is very lower in the region where Major strain is higher. The strain in that region is compressive in nature. The value of the Minor strain is 0.27 which is in at the punch nose radius so it is the critical region where failure can occurs.

Fig: 4.23 Shows the flow limit diagram of the process.

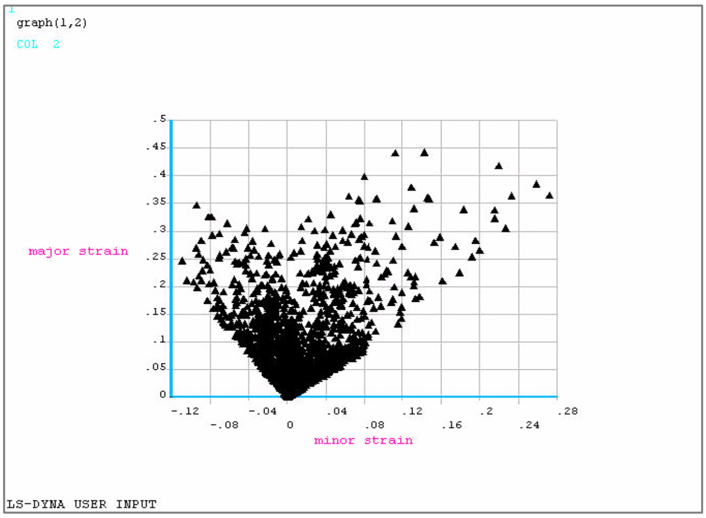

Fig: 4.23 Flow limit diagram of square cup (Aluminum 5052), Die radius 8mm.

Fig: 4.23 Shows that the plane strain condition the value of Major strain is 0.32., which is safe value for the deep drawing of Aluminum 5052. There are some of the points which are falling in the wrinkling limit zone which indicated the wrinkling of the component. Fig: 4.24 Shows the flow limit stress diagram which new trend in the deep drawing process to investigate the process for the more than one draw.

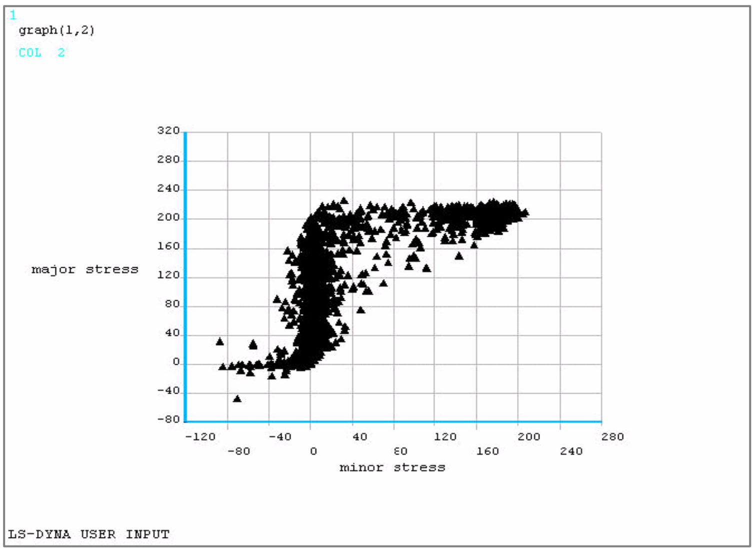

Fig: 4.24 Flow limit stress diagram stress of square cup (Aluminum 5052), Die radius 8mm.

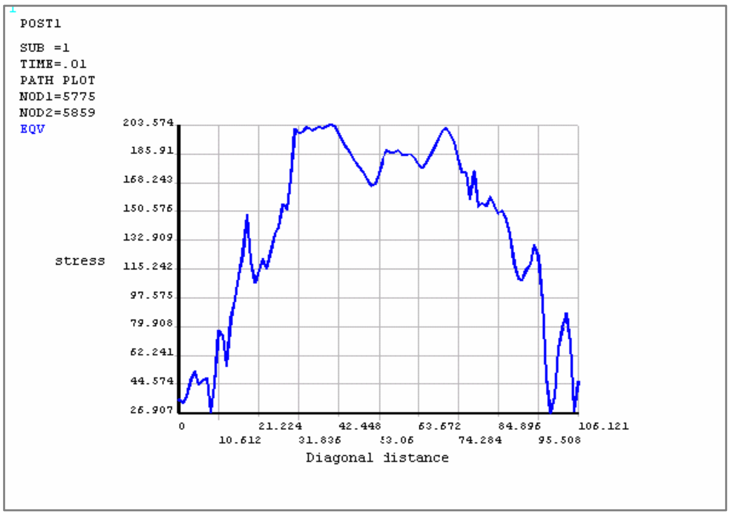

Fig: 4.25 Von mise's equivalent stress along the diagonal direction for the square cup (Aluminum 5052), Die radius 8mm.

Fig: 4.25 Shows that the region of the punch radius it is reaching up to the highest value. Values are lower in the outer contour of the blank. It indicates sharp increase in the stress in region of the clearance.

4.5.3 FEM simulation of square cup of aluminum 5052 for the die radius of 5mm.

The simulated results for the die radius of 5mm are carried out. In The case results are within the strain limits but wrinkles are more. To reduce the wrinkles die radius of 5mm is used for this simulation. Blank holding force is varied between 3700N to 4000N to get the required shape.

Fig 4.26 Shows the result of the Von mises's stress.

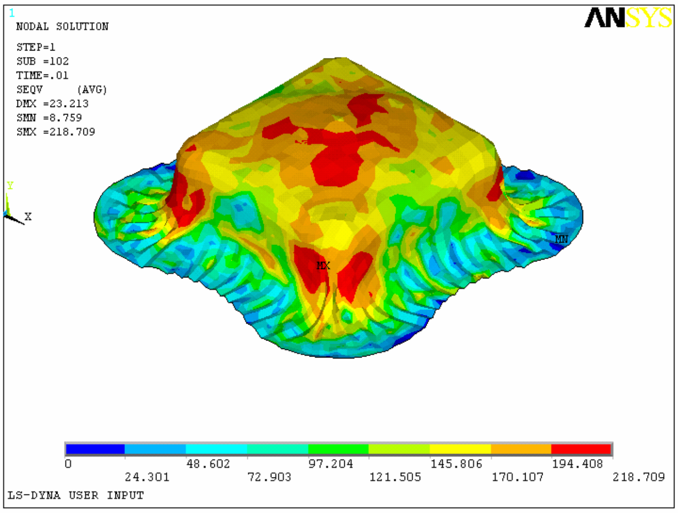

Fig: 4.26 Von mise's equivalent stress produced in square cup (Aluminum 5052), Die radius 5mm.

Fig: 4.26 Shows that maximum value of the stress is 218.7 N/mm^2. In the 8 mm radius case the value was lower. As the radius of the die is decreased the stress in the region just below the die radius is increased. But it is lower than the ultimate stress (265 N/mm^2).

Fig: 4.27 Shows the Major strain produced in the cup.

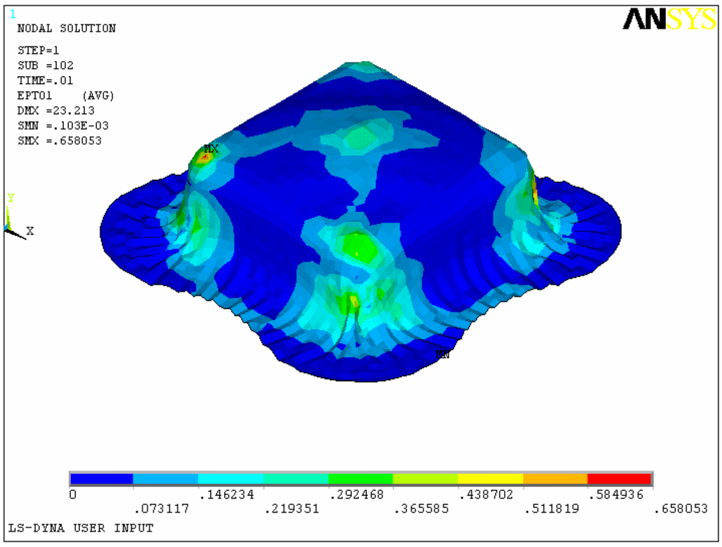

Fig: 4.27 Major strain produced in square cup (Aluminum 5052), Die radius 5mm.

Fig: 4.27 shows that the Major strain is higher in the region die radius. As the die radius is decreased the material flow over the die is decreased and that is creating higher strain value in that region. It is also shows that the strain value is higher than that was in the 8mm radius case.

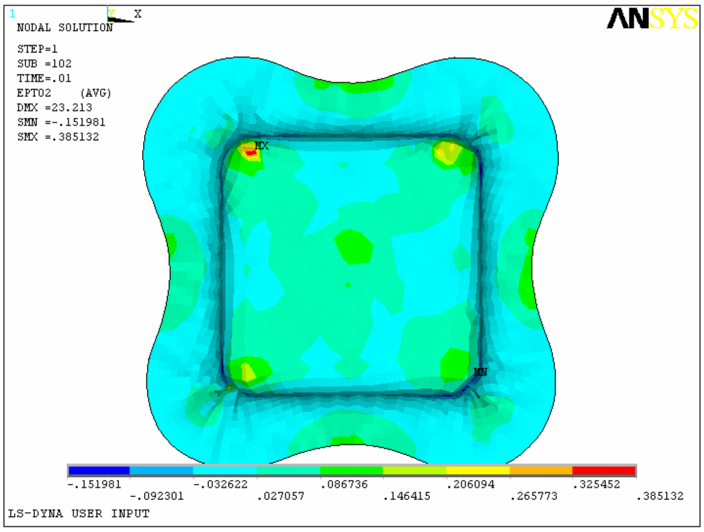

Fig: 4.28 Minor strain produced in square cup (Aluminum 5052), Die radius 5mm.

Fig: 4.28 Shows that the minor strain is lower in the region where the major strain is higher that indicated the deep drawing operation. The maximum value of the strain is 0.38 and min. value of the strain is -0.1519. At the punch nose values are higher due to the bending and unbending of the metal in that region.

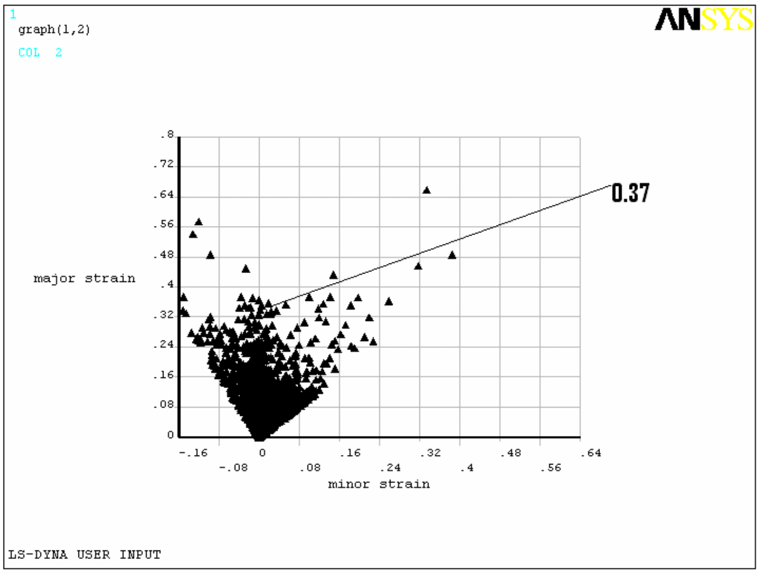

Fig: 4.29 Flow limit diagram of square cup (Aluminum 5052), Die radius 5mm.

Fig: 4.29 Shows the flow limit diagram of the process. The maximum value of the Major strain at the plane strain condition is 0.37, which is safe for the material. Some of the points are falling above wrinkling limit, which indicates wrinkling in the part. Fig: 4.30 Shows the flow stress diagram of the process. It is used when more than one draw is required.

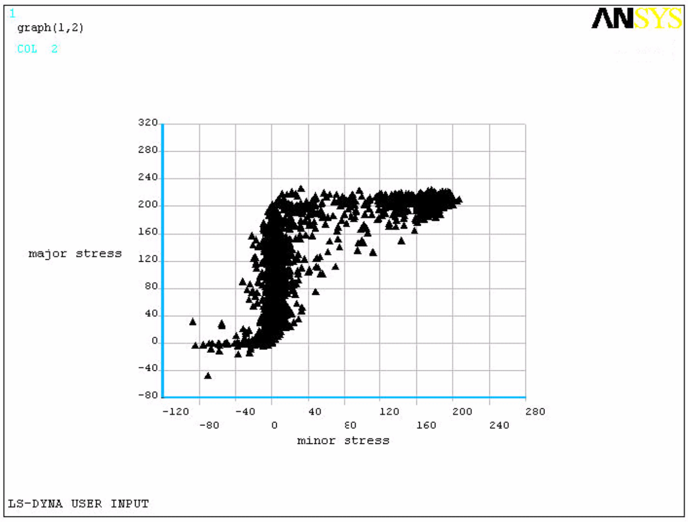

Fig: 4.30 Flow limit stress diagram of square cup (Aluminum 5052), Die radius 5mm.

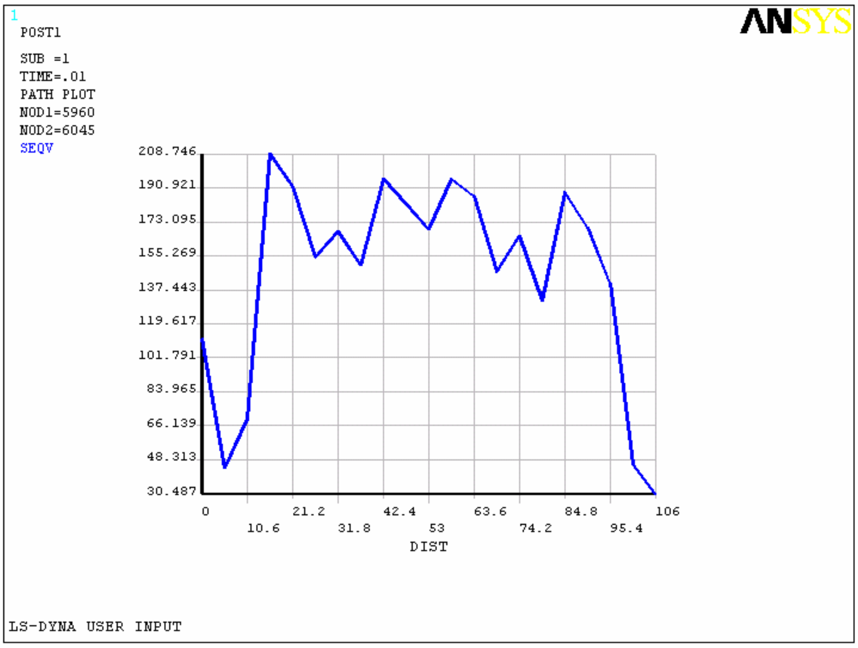

Fig: 4.31 Von mise's equivalent stress along the diagonal direction for the square cup (Aluminum 5052), Die radius 5mm

Fig: 4.30 Shows that there is sharp increase in the stress value than that was in the 8 mm radius case. In the center of the blank stress value is lower.

From the above two cases it can be concluded that, if the die radius is increased amount of wrinkles are very high, but the strain values are less. By decreasing the die radius, wrinkles get reduced, but the strain values are coming higher. There should be optimum die radius within which the wrinkle free components within the permissible safe value of strain can be drawn. In this case 5mm die radius has given better result.

CHAPTER 5

Experimental validation of deep drawn square aluminum 1100 cup

5.1 Introduction

The analysis of the deep drawing process of square aluminum of has been carried out on the mechanical press of the 20 tonnes capacity. The arrangement of the die and punch is in inverted fashion as the displacement is given to the die and punch is in the stationary condition. Die travel is given up to 25 mm. Constant blank holding force is used to prevent the creation of the wrinkles in the part. Grid of the circular shape is marked with the laser on the surface of blank. Measurement of the elongated grid is carried out with the profile projector.

5.2 Experimental set up.

5.2.1 Tooling

The deep drawing tools are made according to the diagram shown in the fig 5.1. The punch size is 48x48x70 mm with the corner edge radii 5 mm and the corner radii in the plane view is taken as 8mm. The die radius is taken as 5 mm. as it is smaller part the radius of the die should be smaller. The corner radius of the die is taken as 10 mm.

Fig: 5.1 Components of the die set

 

Fig: 5.2 Punch plate **Fig: 5.3 Die pate**

Fig: 5.4 Die set assembly

Blank holder size is taken as140x140. Set of the blank holder and floating plate is used which is connected by the four pins. The floating plate is joined with the steel spring (Appendix A) to provide the blank holding force on to the blank. As blank holding set is in floating condition that will apply gradual force on to the blank.

Complete die set with the pillar is shown in fig: 5.4. As the gap is provided in the die plate height of the component can be adjusted up to 5mm. Steel spring assembly with the supporting plate is shown in fig: 5.4. For the application of the blank holding pressure spring is tighten and displacement is given.

Fig: 5.5 Shows the 20 tonnes mechanical press used for the experiment.

Fig: 5.5 Mechanical press of 20 tonnes capacity

5.2.2 Blank preparation

Experiment was carried out with three different blank; square, square with corner radius and circular shapes. The radius provided on the blank with the radii at the corner is 4 to 5 mm less than the initially used in the FEM simulation.

Blanks are marked with the circular grid of the 2.5mm size with evenly spaced at a distance of 0.5 mm. Circular grid marking is shown in the square bank. Only small zone of the marking is shown.

Fig: 5.6 Circular grid marking with the use of laser on the blank

5.3 Experiment of the square aluminum cup.

Four blanks were drawn with the constant blank holding force. The calculated blank holding force which is 2500-2700N is applied with the help of the deflection of the coil spring. Deflection to the spring is given with collar and nut provided in the spring assembly to get the required force. Also as the blank holder is in floating condition, for that deflection of spring up to the cup height is also taken in to the account. As with the above arrangement gradually increasing force was applied on to the blank.

5.3.1 Measurement of strains:

Measurements of strains have been carried out with the help of circular grid analysis. The initial size of the circle is 2.5 mm (0.1 in). Those are evenly spaced at a distance of 0.5 mm. Measurements are taken on the profile projector. Major and minor axes of ellipse are measured and by the standard equation engineering strains are calculated.

$$e_1 = \frac{l_1 - l_o}{l_o}$$

$$e_2 = \frac{l_2 - l_o}{l_o}$$

Where l_1 and l_2 are major and minor axis of the ellipse and e_1 and e_2 are major and minor strains respectively.

Fig: 5.7 Profile projector

5.3.2 Results of the experiment.

The experiment is carried out on the four types of blank; square blank without circular grid, square bank with circular grid, square blank with the corner radius and circular blank

1. Circular blank.

Drawn part with the circular blank is shown in fig. It observed that the metal is reduced in the circular cup the so the gripping area was reduced and due to that strain values are coming in the safe region.

Fig: 5.8 Deep drawn cup with the circular blank

Fig: 5.8 Shows that there circular blank is nearer to the optimum size. As also the strain value are little higher in this case but they are nearer to the simulated results. Blank holder force area is smaller in this case so the strain values are lower. The strain value at the critical region is shown in the table

Measured strains and flow limit diagram are shown below:

Table 5.1: Major and Minor strains for the circular blank. (Aluminum 1100)

Region	Sr. no	Major strain	Minor strain
Around die radius	1.	0.7	-0.352
	2.	0.769	-0.386
	3.	0.488	-0.432
	4.	0.576	-0.32
	5.	0.044	-0.528
	6.	0.016	-0.132
	7.	1.138	-0.58
Punch nose radius	8.	0.356	-0.268
	9.	0.06	-0.112
	10.	0.104	-0.044
	11.	0.072	-0.084

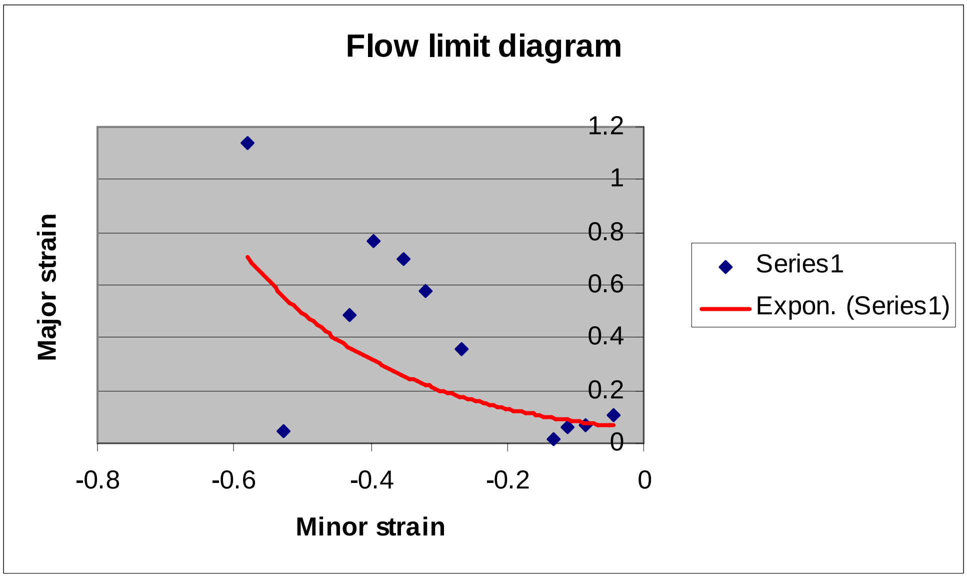

Fig: 5.9 Experimental Flow limit curve for the circular blank. (Aluminum 1100)

2. Square blank with grid marking.

With the grid marking the final drawn part was stretched more at the corner. It was gripped at the die radius and that has created major strain in that zone, which showing the starting of the circumferential failure. The splitting at the corner in the fig 5.10 is shown. Calculate strain value in the drawn part around the corner of failure zone is given in the table 5.1.

Fig: 5.10 Deep drawn cup from the square blank with grid marking

As compare to circular blank in this case more stretching of the material has taken place due to more blank holding contact area. Although there was effect of circular marking on the blank in the circular blank it was not fail due to less blank holding area. But in this case the blank holding force area is higher due to that the strain values are coming higher in the wall of the cup just below the die radius. The values are shown in the table 5.2.

Measured strains and flow limit diagram are shown below:

Table 5.2: Major and Minor strain for square blank (Aluminum 1100)

Region	Sr. no.	Major strain	Minor strain
Just below the die radii	1.	0.76	-0.42
	2.	0.756	-0.484
	3.	0.164	-0.3216
	4.	0.228	-0.4
	5.	0.02	-0.28
	6.	0.224	-0.372
	7.	0.556	-0.336
Flange	8.	0.728	-0.448
	9.	0.696	-0.3
	10.	0.592	-0.424
Punch nose radius	11	0.04	0.032
	12.	0.69	-0.12

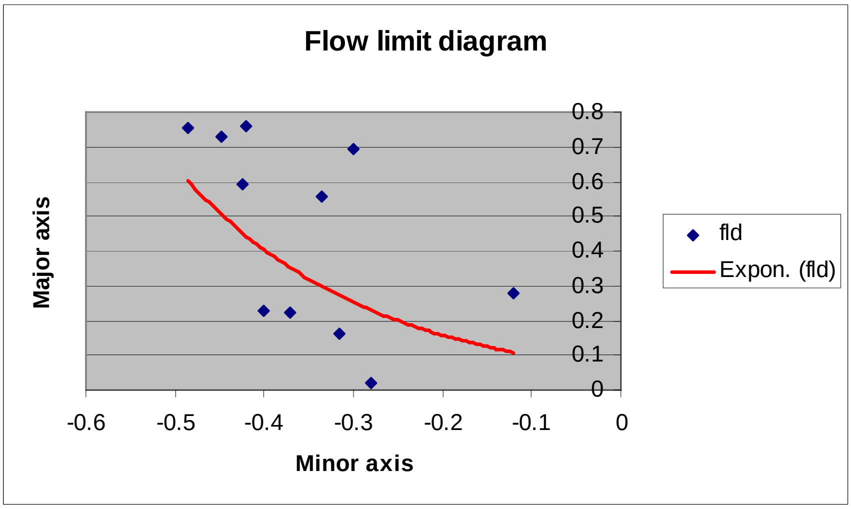

Fig: 5.11 Experimental flow limit curve for the square blank

3. Square blank with the radius provided at the corner.

In the FEM simulation exact corners were made but in the in the actual blank the side cutting is given which having less radius than actual one. Fig 5.12 shows the deep drawn component. It has same type of fracture that was in the earlier one but having less strained that square blank. The strain values were calculated and shown in the table 5.3.

Fig: 5.12 Deep drawn cup form the square blank providing radius at corner.

In this blank the blank holding force is lower than that for the square blank. So strain values are coming lower in than the square blank in the critical region. But as grids are marked deeper at some points the value is crossing very higher limit. So at that point it just starts to fail. Theoretically this shape is the perfect shape for the deep drawing due to the just enough material in the corner region to avoid the wrinkles.

Measured strains and flow limit diagram are shown below:

Table 5.3 major and minor strain for the square rounded blank

Region	Sr. no.	Major strain	Minor strain
Just below the die radii	1.	1.048	-0.412
	2.	0.332	-0.236
	3.	0.824	-0.156
	4.	0.876	-0.356
	5.	0.564	-0.468
	6.	0.104	0.128

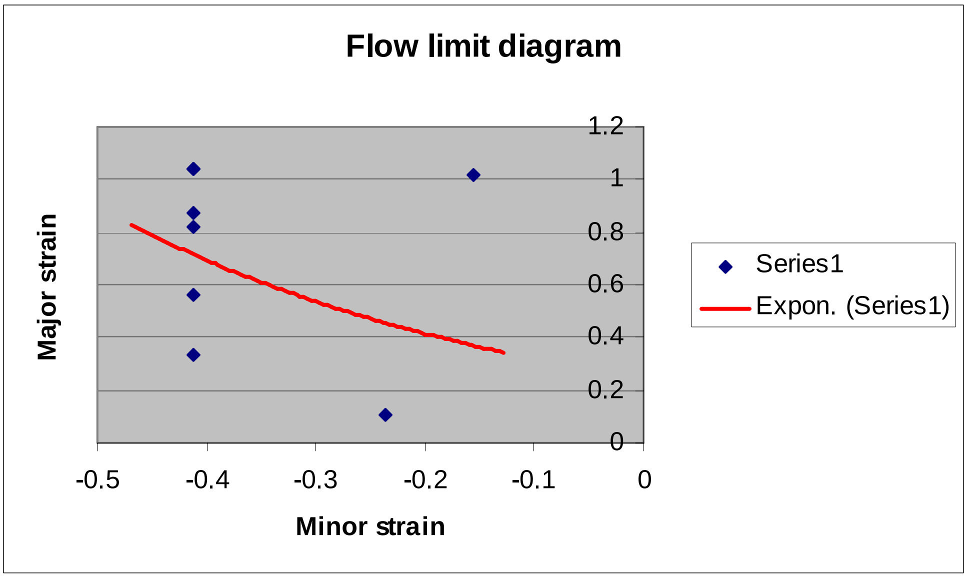

Fig: 5.13 Experimental Flow limit diagram for the deep drawn providing radius at the corner.

4. Square blank without grid marking.

Deep Drawn component with the square blank is shown in the fig: 5.14. As, there is no grid marking on surface of the blank it can able to move easily on to the die radius so there is no earing effect at the wall of the drawn part.

Figure 5.14: Deep drawn aluminum cup from the square blank (Without grid marking)

5.4 Remarks.

The results obtained by the FEM simulation and experimental investigation are compared and it is found that there are many factors which are affecting the deep drawing process which directly or indirectly affects the actual process. As the comparison of the both results shows that the FEM simulation results or major and minor strain values are coming within the standard limiting diagram, but as experimentally found that due to the marking of the grid with the laser the friction or gripping of the surface with die radius was occurred and due to that the strain values at nearer to the die radius was very high. So strain values in the critical region and that was the causes of failure. The simulated and experimental results of circular results are in very good agreement. In the experiment due to the eccentricity of the blank holder pad it is failing at one of the corner.

In the next chapter results discussion at the critical zone is given and comparison of the simulated results with the results is given which provides the pattern of the strains in the critical zones. Also future scope and conclusion are included.

CHAPTER 6

Results and Discussions

6.1 Introduction

In this chapter results and general discussions have been presented. Finally the main conclusion and contributions of the present work are given. Also scope for the future has been suggested.

6.2 Comparisons of Results and discussions

The present work has been carried out to study the different pattern of strain in deep drawn square aluminum cup. There are many processing and material parameters, which are affecting the deep drawing process. Die radius and initial shape of the blank are one of the geometrical parameters which are affecting the strain pattern deep drawn part. Major and minor strains are mostly used for the investigation of the strain pattern. Flow limit curve is used to decide the critical region of the process. In this section comparison of the strain values at the die radius have been carried out.

6.2.1 Comparison of results for the circular blank.

In comparison is carried out at the die corner radius. Comparison of the strain values between simulated results and experimental results are shown below.

Table 6.1: Comparison of the strains for the circular blank.

Sr. no.	Simulated results		Experimental results	
	Major strain	Minor strain	Major strain	Minor strain
1.	0.755	-0.343	0.700	-0.352
2.	0.823	-0.369	0.769	-0.396
3.	0.503	-0.322	0.488	-0.432
4.	0.658	-0.343	0.576	-0.320
5.	0.401	-0.332	0.356	-0.268
6.	0.187	-0.47	0.104	-0.044

From the above results we can say that the simulated results and experimental results are in very good agreement. In the experimental results minor strain at one of the location is coming very high but that is due to the stretching of the surface. Also the minor strains are in agreement with the experimental results. Amount of wrinkles are more than the results of other blanks shape, which are in agreement with the simulated results.

6.2.2 Comparisons of results for square blank.

Comparisons are carried out near the die radius. It is the region where the metal flow over the radius and bending of the metal take place. Below table shows the comparison of the major and minor strains.

Table 6.2: Comparison of the strains for the square blank

Sr. no	Simulated results		Experimental results	
	Major strain	Minor strain	Major strain	Minor strain
1.	0.747	-0..181	0.76	-0.42
2.	0.745	-0.182	0.756	-0.484
3.	0.522	-0.176	0.556	-0.336
4.	0.114	-0.181	0.164	-0.316
5.	0.202	-0.180	0.228	-0.4
6.	0.01	-0.170	0.020	-0.28
7.	0.212	-0.176	0.224	-0.372

Form the above values of the strain we can said that the major strains are almost in agreement with the each other but the difference in the minor strains are there, that is due to the anisotropy of the materials. As pure aluminum of commercial grade is used their anisotropy will be different and that is creating higher minor strain in the components. Also the grids created by laser are little deeper so the gripping of the metal at the die surface was occurred and that is the main reason of failure of the component with the grid marking. Component was failed at one of the corner of the die, that is due to the blank holding force was not uniformly applied on the surface of the blank.

6.2.3 Comparison of results for the square blank provided radius at the corner.

In this also comparison is carried out at the die corner radius. Comparison of the strain values between simulated results and experimental results are shown below.

Table 6.3: Comparison of the strains for the square blank provided radius at the corner

Sr. no	Simulated results		Experimental results	
	Major strain	Minor strain	Major strain	Minor strain
1.	0.187	-0.124	1.048	-0.412
2.	0.152	-0.109	0.332	-0.236
3.	0.183	-0.091	0.824	-0.156
4.	0.186	-0.121	0.876	-0.356
5.	0.156	-0.126	0.564	-0.468

From the above results we can say that component is failed in the experimental. Strain values are not in agreement with each other. The simulated results show that there were small strains just below the die radius. But in the experiment it was failed just below the die radius, because of the friction crated due to the grid. Maximum value of the major strain is very high. But the crack was smaller than that was in the square blank. That was due to the smaller blank holding contact area of the blank. With the radius provided at the blank, binder force area was reduce so, effect of higher friction between the die and blank was balanced. But the wrinkles were more due to the reduced in the binder force area.

CHAPTER 7

Overall Conclusion and scope for Future work

7.1 Introduction

In this proposed thesis study of deep drawn aluminum cup by taking different geometry of the blank has been carried out. FEA simulations have been carried out in LS-DYNA .Explicit dynamic analysis is helpful tool to carry out the study of the strain pattern. Square aluminum cup with the three different initial blank shapes were simulated.

Also use of R_{off} value has given quite satisfactory result for finding the Blank holding force for the 3D simulation. Macro in the ANSYS parametric design language (APDL) is quite useful for reducing the simulation time.

Experimental results were found in good agreement with the simulated results. The simulated and experimental results of circular blank are in very good agreement. For the other two cases experimental results of strain value are little higher than the simulated results due to the effect of circular grid marking.

7.2 Conclusions

The conclusions of the thesis are as follows.

1 The R_{off} to find the blank holding force was used, which can be used for the complicated geometry also and it is useful for getting the initial blank holding force required for the 3D simulation.

2 The simulated results and experimental results were found in very good agreement in the circular blank. Square blank and square blank with corner radius having higher contact area than the circular blank so the strain values were higher in that two cases. Also due to the circular grid marking friction between the die and blank was increased, which has created higher strain just below the die radius. Although, with effect of grid marking simulated results and experimental results were found in very good agreement in the circular blank.

3 Novel method is adopted for marking the grid pattern, it is observed that grid are marked deeper and it adversely affect the strain pattern and eventually failure at critical points has been found.

4 Even with deeper grid marking experimental results of circular blank is in very good agreement with simulated results.

5 Macro with ANSYS parametric design language (APDL) has been developed for simulation and is found very helpful in order to expedite simulation iterations. The simulations were carried out varying parameters with the use of Macro.

7.3 Scope for future work.

1. Optimization of parameters required for the process can be carried out with the help of ANSYS parametric design language (APDL).
2. Laser marking can be used for the marking of the circular grid on the blank. It easy and accurate method of marking.
3. Topological optimization of the blank can be done to get the optimum blank shape.

Appendix A

1 Hill 48 yield criteria.

$$2f(\sigma_{ij}) = F(\sigma_y - \sigma_z)^2 + G(\sigma_z - \sigma_x)^2 + H(\sigma_x - \sigma_y)^2$$
$$+ 2L\tau_{yz}^2 + 2M\tau_{zx}^2 + 2N\tau_{xy}^2 = 1$$

2. Hill 90 yield criteria.

$$f(\sigma_{ij}) = |\sigma_x + \sigma_y|^m + (\sigma_b^m/\tau^m)|(\sigma_x - \sigma_y)^2 + 4\tau_{xy}^2|^{m/2}$$
$$+ |\sigma_x^2 + \sigma_y^2 + 2\tau_{xy}^2|^{(m/2)-1}\{-2a(\sigma_x^2 - \sigma_y^2)$$
$$+ b(\sigma_x - \sigma_y)^2\}$$
$$= (2\sigma_b)^m$$

3.Hill 93 yield criteria.

$$\frac{\sigma_1^2}{\sigma_0^2} - \frac{c\sigma_1\sigma_2}{\sigma_0\sigma_{90}} + \frac{\sigma_2^2}{\sigma_{90}^2} + \left\{(p+q) - \frac{(p\sigma_1 + q\sigma_2)}{\sigma_b}\right\}\frac{\sigma_1\sigma_2}{\sigma_0\sigma_{90}} = 1$$

where

$$\frac{c}{\sigma_0\sigma_{90}} = \frac{1}{\sigma_0^2} + \frac{1}{\sigma_{90}^2} - \frac{1}{\sigma_b^2}$$

$$p = \left[\frac{2r_0(\sigma_b - \sigma_{90})}{(1+r_0)\sigma_0^2} - \frac{2r_{90}\sigma_b}{(1+r_{90})\sigma_{90}^2} + \frac{c}{\sigma_0}\right]\frac{1}{\frac{1}{\sigma_0} + \frac{1}{\sigma_{90}} - \frac{1}{\sigma_b}}$$

$$q = \left[\frac{2r_{90}(\sigma_b - \sigma_{90})}{(1+r_{90})\sigma_{90}^2} - \frac{2r_0\sigma_b}{(1+r_0)\sigma_0^2} + \frac{c}{\sigma_{90}}\right]\frac{1}{\frac{1}{\sigma_0} + \frac{1}{\sigma_{90}} - \frac{1}{\sigma_b}}$$

4. Material properties aluminum 5052

Compositions: 2.5% magnesium, 0.25% chromium

Mechanical properties:

Ultimate tensile strength	265 MPa
Tensile yield strength	214 MPa
Modulus of elasticity	73G Pa
Shear modulus	25.9 Gpa
Poisson ratio	0.33
R_0	0.78
R_{45}	0.68
R_{90}	0.65
Barlat's index	11

5. Material properties for aluminum 1100

Mechanical properties:

Ultimate tensile strength	108 MPa
Yield strength	80 MPa
Young modulus	71000MPa
Strength coefficient	151.3MPa
Hardening index	0.254
R_0	0.681
R_{45}	0.513
R_{90}	0.612
Barlat index	11

6. Specifications of steel spring

Mean diameter of coil spring (D)	70mm
Free length of the spring (L)	241.3 mm
Wire die meter (d)	10mm
Modulus of rigidity (G):	210KN/mm^2
No. of coils.(n)	12
Pitch	22
Stiffness of the spring	24.29 N/mm

Appendix B

Macro for the FEM simulation in ANSYS parametric design language.

```
prep7
ET,1,SHELL163                  !Defining shell 163 element for the die, punch, blank
holder, and blank.
!*
KEYOPT,1,1,5
KEYOPT,1,2,0
KEYOPT,1,3,0
KEYOPT,1,4,5,
!*
!*
ET,2,SHELL163
!*
KEYOPT,2,1,5
KEYOPT,2,2,0
KEYOPT,2,3,0
KEYOPT,2,4,5,
!*
ET,3,SHELL163
!*
KEYOPT,3,1,5
KEYOPT,3,2,0
KEYOPT,3,3,0
KEYOPT,3,4,5,
!*
ET,4,SHELL163
!*
KEYOPT,4,1,5
KEYOPT,4,2,0
KEYOPT,4,3,0
KEYOPT,4,4,5,
!*
!*
*SET,_RC_SET,1,                !Defining the real constant for the above set.
R,1
RMODIF,1,1,1,1,1,1,1,1,
!*
RMODIF,1,8,1
!*
*SET,_RC_SET,2,R,2
RMODIF,2,1,1,1,1,1,1,1,
!*
RMODIF,2,8,1
!*
*SET,_RC_SET,3,
```

```
R,3
RMODIF,3,1,1,1,1,1,1,1,
!*
RMODIF,3,8,1
!*
*SET,_RC_SET,4,
R,4
RMODIF,4,1,1,1,1,1,1,1,
!*
RMODIF,4,8,1
!*
!*
MP,DENS,1,2600e-9            !Input parameters for the Barlat's 3 parameter model.
MP,EX,1,71000
MP,NUXY,1,.34
TB,PLAW,1,,,3,
TBDAT,1,1
TBDAT,2,151
TBDAT,3,80
TBDAT,4,11
TBDAT,5,.78
TBDAT,6,.67
TBDAT,7,.56
TBDAT,8,0
!*
EDMP,RIGI,3,0,0           !Defining material property for Blank holder.
MP,DENS,3,7500e-9
MP,EX,3,2e5
MP,NUXY,3,.3
!*
EDMP,RIGI,4,0,0           !Defining material property for Die.
MP,DENS,4,7500e-9
MP,EX,4,2e5
MP,NUXY,4,.3
!*
EDMP,RIGI,2,0,0           !Defining material property for punch.
MP,DENS,2,7500e-9
MP,EX,2,2e5
MP,NUXY,2,.3


/PREP7                  !Meshing of the different components.
AESIZE,all,2,
TYPE,   1               !Meshing of blank with element  size 2
MAT,   1
REAL,  1
ESYS,   0
SECNUM,
!*
AMESH,129
```

```
!*
TYPE,   2                  !Meshing of Punch
MAT,   2
REAL,   2
ESYS,    0
SECNUM,
!*
AMESH,154,160,2
!*
TYPE,   4                 !Meshing of Die
MAT,   4
REAL,   4
ESYS,     0
SECNUM,
!*
AMESH,195,211,
!*
TYPE,   3                 !Meshing of Blank holder
MAT,    3
REAL,   3
ESYS,       0
SECNUM,
!*
AMESH,107,128,
!*
  /GO
D,5735, ,0, , , ,ALL, , , , ,  !Applying constraint on die
ALLSEL,ALL
EPLOT
FINISH
/PREP7
!*
EDPART,CREATE                  !Creating part ID for the different components.
!*
EDCGEN,FSTS,4,1,0.12,0.1,0,0,0, , , , ,0,10000000,0,0 !Defining surface to surface
forming contacts.
!*
EDCGEN,FSTS,4,2,0.12,0.1,0,0,0, , , , ,0,10000000,0,0
!*
EDCGEN,FSTS,4,3,0.12,0.1,0,0,0, , , , ,0,10000000,0,0
!*
FINISH
/SOL
*DIM,time1,ARRAY,2,1,1, , ,    !Defining array parameters for time.
!*
*SET,TIME1(1,1,1) , 0.00
*SET,TIME1(2,1,1) , 0.001
*DIM,time,ARRAY,4,1,1, , ,     .
!*
*SET,TIME(1,1,1) , 0.00
```

```
*SET,TIME(2,1,1) , 0.001
*SET,TIME(3,1,1) , 0.009
*SET,TIME(4,1,1) , 0.01
*DIM,load,ARRAY,4,1,1, , ,
!*
*SET,LOAD(1,1,1) , 0          !Punch load velocity or displacement.
*SET,LOAD(2,1,1) , 2000
*SET,LOAD(3,1,1) , 2000
*SET,LOAD(4,1,1) , 0
!*
*SET,BLANHOLDER(1,1,1) , 0                 !Blank holding force load .
*SET,BLANKHOLDER(2,1,1) , 3500
*SET,BLANKHOLDER(3,1,1) , 3500
*SET,BLANKHOLDER(4,1,1) ,
!*
EDLOAD,ADD,RBFY,0,   2,TIME,BLANKHOLDER, 0, , , , ,   !Applying load on
blank holder.

EDLOAD,ADD,RBVY,0,    2,TIME,LOAD, 0, , , , ,           !Applying load on
Punch(velocity curve)

TIME,0.01,                   !define solution time
ALLSEL,ALL
SAVE

FINISH
```

References

1) ASM handbook Volume 14 (Forming and forging).

2) I. Dejmal, J. Tirosh, A. Shirizly, L. Rubinsky,
"On the optimal die curvature in deep drawing processes", International journal of mechanical science 44 (2002) 1245-1258.

3) Tool and die design. by Prakashkumar.

4) Hoon Huh, Tae Hoon Choi
"Modified membrane Finite element formulation for sheet metal forming analysis of planar anisotropic materials", International Journal of Mechanical Sciences 42 (1999) 1623-1643.

5) Rahul K. Verma, Sanjay Chandra
"An improved model for predicting limiting drawing ratio." Journal of materials processing Technology 172(2006)218-224.

6) Yasuo Marumo , Hiroyuki Saiki , Toshihiko Mori
"Combined effects of strain hardening characteristics and toolgeometry on the deep-drawability of square aluminum cups", Journal of material processing technology80-90 (1999).

7) S.G. Desai, P.P. Date
"On the quantification of strain distribution in drawn sheet metal products" Journal of Materials Processing Technology 177 (2006) 439–443.

8) Hong Yao, Jian Cao.
"Assessment of Corner Failure Depths in the Deep Drawing of 3D PanelsUsing Simplified 2D Numerical and Analytical Models."

9) L Wang, T.C. Lee
"The effect of yield criteria on the forming limit curve prediction and deep drawing process simulation.", International journal of tools and manufacturing. 46 (2006) 988-995.

10) J.W. Yoon, F. Barlat, and R.E. Dick, S. Choudhry
"Prediction of Eight Ears in Drawn Cup Based on a New Anisotropic Yield Function."

11) Jaachim Panckert,

"Experimental investigation of a square cup deep drawing process ", Journal of material processing technology (1995) 375-384.

12) Claes Arvidson,

"Numerical simulation of sheet metal forming for high strength steels ", Journal of material processing technology (2005) 423-434.

13) M. Samual,

"Numerical and experimental investigation of forming limit diagram in sheet metals", Journals of material processing and technology (2004) 424-431.

14) Hong Yao, Brad L. Kinsey, Jian Cao.

"Rapid design of corner restraining force in deep drawn rectangular parts", International Journal of Machine Tools & Manufacture 40 (2000) 113–131

15) John O. Hallquist.

LS-DYNA Theoretical manual, Livemore software technology corporation 1998.

16) Metal forming science and engineering by Edward M. Mielnik.

17) Metal forming and finite element methods by Kobayashi Haltan.